AD-A155 379

AFGL-TR-84-0318

EFFECTS OF HYDROMETEORS ON ELECTROMAGNETIC WAVE PROPAGATION

John F. Ebersole
Wai K. Cheng
John Hallett
Robert G. Hohlfeld

Creative Optics, Inc.
25 Washington Street
Bedford, Massachusetts 01730

Final Report
June 1984-December 1984

January 1985

Approved for public release; distribution unlimited

DTIC FILE COPY

DTIC
ELECTE
JUN 25 1985
S D
B

AIR FORCE GEOPHYSICS LABORATORY
AIR FORCE SYSTEMS COMMAND
UNITED STATES AIR FORCE
HANSCOM AFB, MASSACHUSETTS 01731

85 06 10 113

"This technical report has been reviewed and is approved for publication"

Morton Glass

MORTON GLASS
Contract Manager

Arnold A. Barnes Jr.

ARNOLD A. BARNES, JR., Chief
Cloud Physics Branch

FOR THE COMMANDER

Robert A. McClatchey

ROBERT A. McCLATCHEY, Director
Atmospheric Sciences Division

This report has been reviewed by the ESD Public Affairs Office (PA) and is releasable to the National Technical Information Service (NTIS).

Qualified requestors may obtain additional copies from the Defense Technical Information Center. All others should apply to the National Technical Information Service.

If your address has changed, or if you wish to be removed from the mailing list, or if the addressee is no longer employed by your organization, please notify AFGL/DAA/LYC, Hanscom AFB, MA 01731. This will assist us in maintaining a current mailing list.

Unclassified
SECURITY CLASSIFICATION OF THIS PAGE

REPORT DOCUMENTATION PAGE

1a. REPORT SECURITY CLASSIFICATION Unclassified	1b. RESTRICTIVE MARKINGS
2a. SECURITY CLASSIFICATION AUTHORITY	3. DISTRIBUTION/AVAILABILITY OF REPORT Approved for public release; distribution unlimited
2b. DECLASSIFICATION/DOWNGRADING SCHEDULE	
4. PERFORMING ORGANIZATION REPORT NUMBER(S) COI-SR-15	5. MONITORING ORGANIZATION REPORT NUMBER(S) AFGL-TR-84-0318
6a. NAME OF PERFORMING ORGANIZATION Creative Optics, Inc. 6b. OFFICE SYMBOL (If applicable)	7a. NAME OF MONITORING ORGANIZATION
6c. ADDRESS (City, State and ZIP Code) 25 Washington Street Bedford, Massachusetts 01730	7b. ADDRESS (City, State and ZIP Code)
8a. NAME OF FUNDING/SPONSORING ORGANIZATION Air Force Geophysics Laboratory 8b. OFFICE SYMBOL (If applicable)	9. PROCUREMENT INSTRUMENT IDENTIFICATION NUMBER F19628-84-C-0115
8c. ADDRESS (City, State and ZIP Code) Hanscom AFB, Massachusetts 01731 Monitor/Morton Glass/LYC	10. SOURCE OF FUNDING NOS. PROGRAM ELEMENT NO.: 62101F PROJECT NO.: 6670 TASK NO: 12 WORK UNIT NO.: DC
11. TITLE (Include Security Classification) Effects of Hydrometeors on Electromagnetic Wave Propagation	
12. PERSONAL AUTHOR(S) John F. Ebersole, Wai K. Cheng, John Hallett, and Robert G. Hohlfeld	
13a. TYPE OF REPORT Final 13b. TIME COVERED FROM JUN 84 TO DEC 84	14. DATE OF REPORT (Yr., Mo., Day) January 1985 15. PAGE COUNT 77
16. SUPPLEMENTARY NOTATION	
17. COSATI CODES FIELD / GROUP / SUB. GR.	18. SUBJECT TERMS (Continue on reverse if necessary and identify by block number) Microwave, Millimeter wave, Radio wave, Infrared, Visible, Ultraviolet, X-ray, EHF, SHF, Rain, Snow, Cloud, Fog, Attenuation, Transmission, Scattering, absorption, Propagation,

(Over)

19. ABSTRACT (Continue on reverse if necessary and identify by block number)

Attenuation of electromagnetic (EM) waves by Hydrometeors such as rain, snow, clouds, and fog, can cause serious degradation of EM wave systems. This report describes such attenuation of radio waves to X-rays, with primary applications to communications in the microwave and millimeter wave portions of the EM spectrum.

(required to include!)

20. DISTRIBUTION/AVAILABILITY OF ABSTRACT UNCLASSIFIED/UNLIMITED ☒ SAME AS RPT ☐ DTIC USERS ☐	21. ABSTRACT SECURITY CLASSIFICATION Unclassified
22a. NAME OF RESPONSIBLE INDIVIDUAL Morton Glass	22b. TELEPHONE NUMBER (Include Area Code) (617) 861-2946 22c. OFFICE SYMBOL LYC

DD FORM 1473, 83 APR EDITION OF 1 JAN 73 IS OBSOLETE

SECURITY CLASSIFICATION OF THIS PAGE

Unclassified

SECURITY CLASSIFICATION OF THIS PAGE

Block 18 (Contd)

Atmosphere, Electromagnetic wave, Hydrometeor

DTIC
ELECTE
JUN 2 5 1985
S D
B

Accession For
NTIS GRA&I ☑
DTIC TAB ☐
Unannounced ☐
Justification
By
Distribution/
Availability Codes
Avail and/or
Dist Special
A-1

SECURITY CLASSIFICATION OF THIS PAGE

TABLE OF CONTENTS

CHAPTER		PAGE
	ACKNOWLEDGEMENTS	iv
1	INTRODUCTION	1
2	PROGRAM OBJECTIVES	5
3	THE AFGL/CSU CLOUD MODEL	6
	3.1 MODEL OUTPUTS	6
	3.2 THE EOSAEL CLOUD TRANSMISSION MODEL CLTRAN	7
4	PROPAGATION ISSUES	11
	4.1 ATTENUATION DUE TO GASEOUS ABSORPTION	12
	4.2 HYDROMETEORS	14
	4.2.1 ATTENUATION MODELLING	15
	4.2.2 OPTICAL CONSTANTS	19
	4.2.3 SIZE DISTRIBUTION	19
5	OVERALL ATTENUATION RESULTS	34
6	MILLIMETER WAVE AND MICROWAVE WAVE PROPAGATION	42
	6.1 DEPOLARIZATION	44
	6.2 SCINTILLATION	48
	6.3 BANDWIDTH COHERENCE	50
	6.4 RAIN ATTENUATION STATISTICS	50
7	X-RAY PROPAGATION	54
	7.1 SUMMARY	54
	7.2 X-RAY PROPAGATION ISSUES	54
8	RECOMMENDATIONS	61
	8.1 BACKGROUND	61
	8.2 PATH LENGTH ABSORPTION MEASUREMENTS	61
	8.3 COMPUTATIONS	65
9	REFERENCES	67
	APPENDIX. X-RAY ABSORPTION COEFFICIENT OF AIR	73

ACKNOWLEDGMENTS

This report was prepared under Contract No. F19628-84-C-0115, Contract Monitor: Mr. Morton Glass of the Air Force Geophysics Laboratory.

Important technical discussions with Mr. Glass, and with Dr. Arnold Barnes, Mr. Vernon Plank, and Dr. Robert Banta, all of AFGL, are gratefully acknowledged. Dr. Vincent Falcone, Jr., provided ideas and suggestions which have greatly benefited this report.

The authors extend a note of appreciation to Dr. Ahmad Torabi for assistance in conducting the literature search, Dr. Leonard Winchester for technical discussions, Ms. Ingrid A. Ebersole for graphic arts support, and Ms. Barbara Vannah for technical typing services.

1. INTRODUCTION

The U.S. Air Force Geophysics Laboratory (AFGL) is involved with a mesoscale modelling effort to characterize the atmosphere from a predictive viewpoint. One model of interest is the one developed by Colorado State University (CSU) and which is now operational at AFGL.

One goal of the AFGL mesoscale modelling effort is to provide the Air Force with a capability for real-time forecasting of mesoscale (approximately 30km x 30km area) weather patterns as they pertain to tactical and strategic scenarios, such as the weather pattern shown in Figure 1-1. In either scenario, the Air Force needs to know the capability of multispectral systems to penetrate adverse weather and aerosols, specifically clouds, fogs, and precipitation.

This report addresses electromagnetic (EM) wave attenuation by the atmosphere for X-rays, ultraviolet (UV) light, visible light, infrared (IR), millimeter waves (MMW), and microwaves (MW). The EM spectrum is shown as Figure 1-2. The primary application of this report is communication attenuation, which affects selection of optimum communication bands, evaluation of channel communication capacity, and identification of possible new high-speed communication bands. For example, covert communication might be achieved near high-attenuation bands, whereas high-speed communication would be done in low-attenuation bands. Other applications include

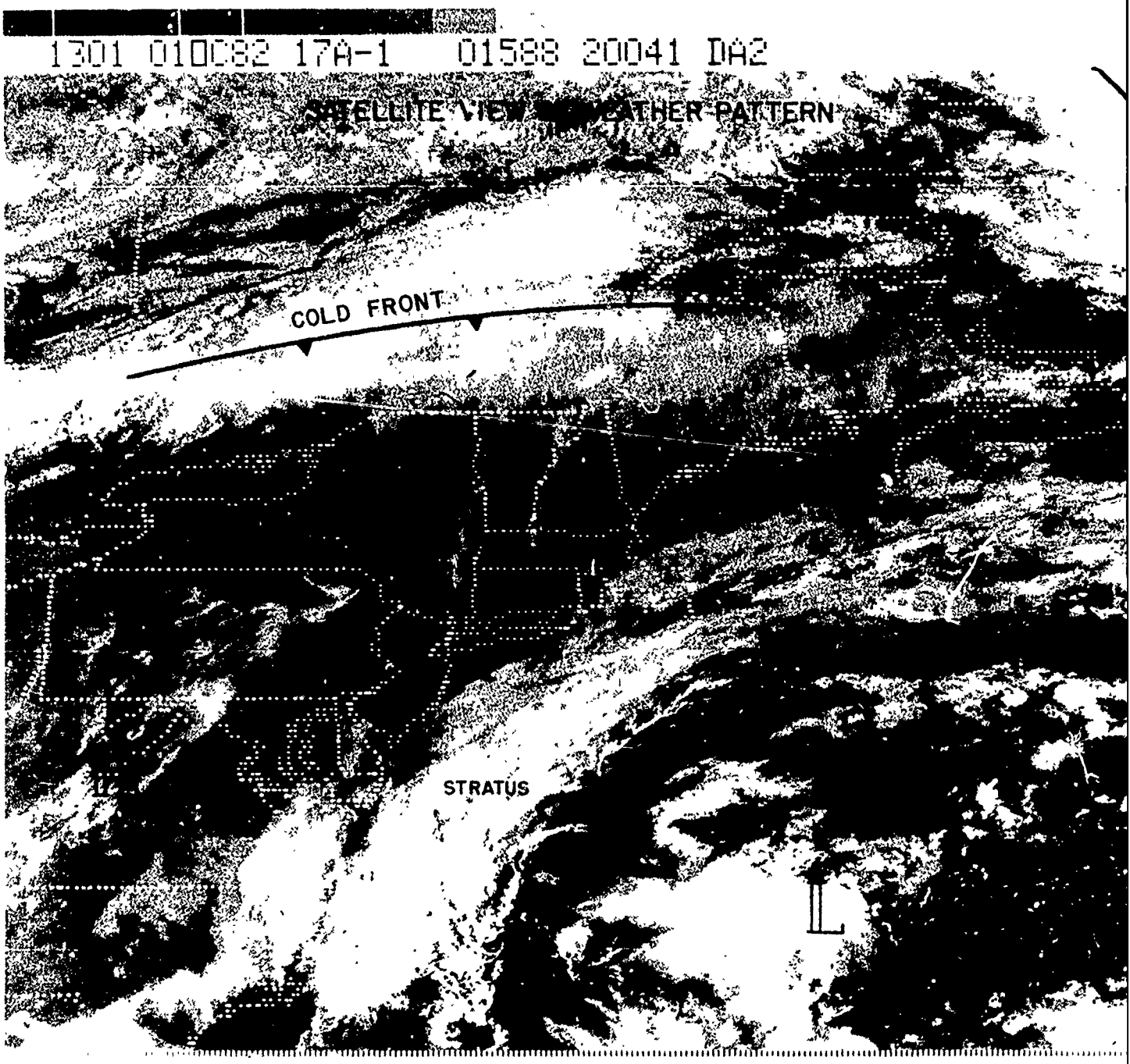

Figure 1-1. Satellite view of weather pattern. Both clouds and fogs are evident. Noteworthy are the "dendritic valley fogs" and cirrus clouds in Pennsylvania and New York. (Personal communication from J. Jiusto, 1983)

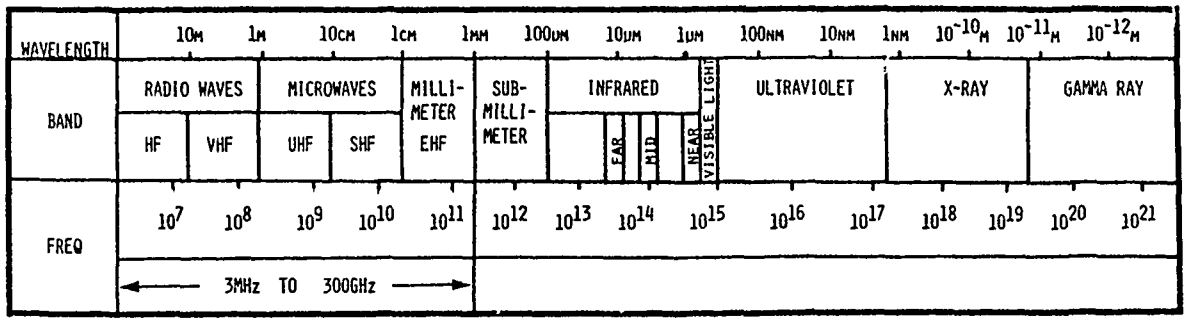

Figure 1-2. The electromagnetic spectrum from radio waves to gamma rays. This report addresses microwaves to X-rays, with emphasis on millimeter waves.

visibility studies, laser designator and smart weapon performance assessments, and directed energy weapon calculations.

It is also an Air Force interest to establish optimum viewing wavelengths or combinations of wavelengths for target acquisition. This will permit long-range (e.g., satellite) observation of targets of interest in current peace-keeping missions as well as in time of war. Further, target detection, recognition, and identification (e.g., from low-flying, fixed-wing aircraft) through atmospheres degraded by adverse weather represents a serious challenge to current and future sensor systems.

At present, the AFGL/CSU model does not have multispectral attenuation calculation capabilities. This report describes a suggested technical approach to the problem of incorporating an attenuation subroutine to the large AFGL/CSU model. This approach is also applicable to other potential cloud/fog models of interest. Also discussed are potential uses of the subroutine and their applications to the solution of Air Force tactical and strategic problems.

2. PROGRAM OBJECTIVES

The objective of this report is to provide recommendations for incorporating a subroutine in the AFGL/CSU mesoscale model in order to calculate EM wave attenuation by clouds, fog, and precipitation in terms of signal strength and signal quality. As mentioned above, this report addresses attenuation of microwaves through X-rays. However, special emphasis is placed on millimeter waves because of increasing Air Force interest in this band.

To achieve this obective, this report addresses the requirements for calculating attenuation through two-dimensional (2D) and 3D structured clouds, since one of the main features of the AFGL/CSU model is its ability to compute 2D and 3D cloud characteristics.

3. THE AFGL/CSU CLOUD MODEL

3.1 Model Outputs

The meteorological information for the attenuation computation is based on the cloud model developed at the Colorado State University (CSU) (Ref. 1). This is a 3D model incorporating mesoscale turbulent transports and meteorological dynamics and is capable of treating irregular terrains. The model treats the water content in the atmosphere by following the evolution of the vapor, liquid, and ice phases, using appropriate submodels for accretion, nucleation, melting, freezing, evaporation, riming, and precipitation. The outputs of interest of the model are the mass loadings of these particles. The mass loading is given by the model in terms of mixing ratios. The following notation applies:

γ_t = total mixing ratio of water substance

γ_v = mixing ratio of water vapor

γ_c = mixing ratio of cloud droplets

γ_r = mixing ratio of rain drops

γ_i = mixing ratio of ice crystals

γ_g = mixing ratio of graupel

The mass loading of the total water content is

$$\rho_t = \gamma_t \rho_a$$

where ρ_a is the density of dry air. The mass loading of the

other components is determined similarly. The total mixing ratio is:

$$\gamma_t = \gamma_v + \gamma_c + \gamma_r + \gamma_i + \gamma_g$$

The distinction between the rain drop and cloud droplets made in the model is that the size of the latter is very small and is assumed to have negligible terminal velocity as well as to have instantaneous evaporation and condensation to maintain supersaturation.

The output of the meteorological model is a spatial distribution of the mixing ratios and ρ_a as a function of time. A typical output is shown in Figure 3-1. For each time frame, therefore, the mass loading distribution of the airborne particles may be calculated for use as input to our recommended attenuation module.

3.2 The EOSAEL Cloud Transmission Model CLTRAN

It is instructive to compare aspects of the AFGL/CSU model with aspects of the cloud attenuation model in the Electro-Optical Systems Atmospheric Effects Library (EOSAEL), a computer library developed by the U. S. Army Atmospheric Sciences Laboratory (Ref. 2). EOSAEL is comprised of 18 empirical, semi-empirical, and theoretical codes, or modules,

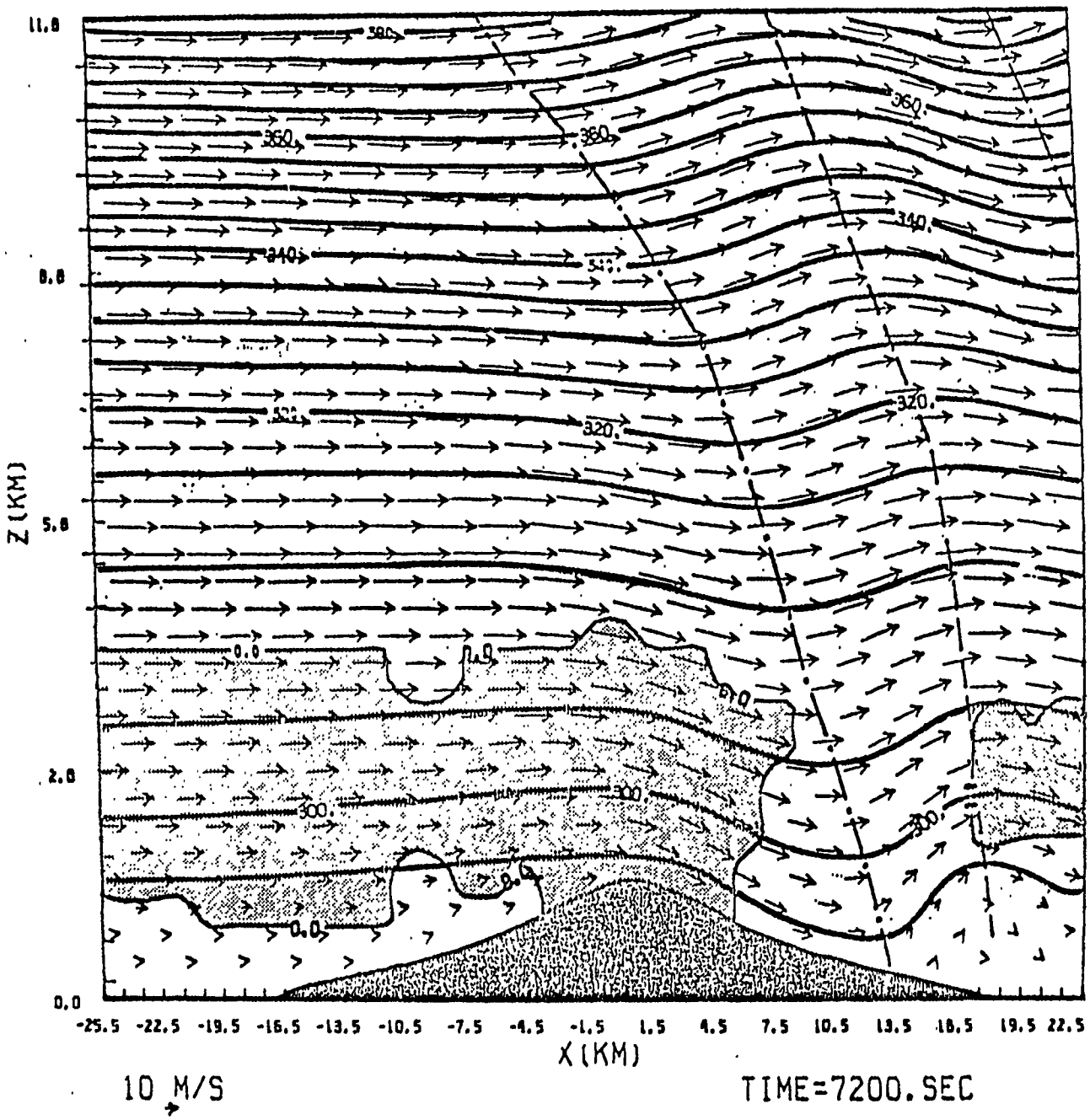

Figure 3-1. Typical output of CSU Meteorological Model. The figure shows a time frame of a cross-section through a simulated orographic cloud. The shaded areas represent regions containing cloud water or ice crystals, and the solid dark area at the bottom of the figure is the terrain. (From Ref. 2.)

that deal with the various aspects of electromagnetic wave propagation under varying atmospheric conditions. Specifically, EOSAEL modules can be used to calculate propagation effects for transmission through natural obscurants (clouds, rain, snow, fog) and battlefield aerosols (smokes, dust, explosions) under a variety of user-selectable conditions. Climatological (probability of occurrence) information for different European and Mideast locations is also included in EOSAEL.

The cloud transmission model of EOSAEL--CLTRAN--calculates slant path transmission through six cloud types for the ultraviolet, visible, and infrared wavelengths. CLTRAN does not calculate millimeter wave or microwave attenuation. CLTRAN uses a one-dimensional (1D) inhomogeneous cloud model. That is, cloud microphysical and optical properties are assumed to vary only as a function of height. These 1D vertical profiles are based upon averages for the six different types of clouds obtained over many years of measurements. Optical transmission is calculated based upon mean particle (droplet) sizes profiles. All particles are considered to be water, rather than a mixture of water and ice particles.

The EOSAEL description for their CLTRAN cloud model emphasizes their statistical approach to cloud modelling. It

has the advantage that 1D (vertical) variations in cloud and droplet properties can be used as a "package" for users. For those applications where 2D or 3D cloud variations occur, such as horizontal orographic cloud changes produced by mountains, CLTRAN is not the appropriate answer, nor was it meant to be. For example, Ref. 3 has noted differences between CLTRAN results and computations in selected situations. Rather, for those applications where a reference atmosphere can be utilized and where no horizontal variations in the cloud are important, CLTRAN can provide information on transmission for visible to infrared wavelengths. For those clouds which have an ice content, or which vary in horizontal directions, or for applications where microwave transmission is important, another approach is needed.

The AFGL/CSU computer cloud model can present 2D and 3D answers to solid/liquid/gaseous water content in clouds. The effects of nucleation from the vapor, melting, freezing, accretion, evaporation and riming are determined from cloud properties and ambient environment conditions (temperature and relative humidity). This deterministic approach (versus the statistical approach of EOSAEL CLTRAN) can be directly applied to all weather conditions and local terrain variations. However it is still necessary to add to the AFGL/CSU computer code an attenuation calculation capability at various wavelengths.

4. PROPAGATION ISSUES

The issues of interest to the evaluation of EM wave transmission in the atmosphere include attenuation, (i.e., the sum of absorption and scattering), depolarization, scintillation, and dispersion (Ref. 4). Depending on the applications, these effects take different levels of importance. In general, for communication purpose, the higher the information content (e.g., bandwidth) carried by the EM wave, the more severe will be the atmospheric effects.

It should be noted that the attenuation effect is, in a sense, of a different nature than the depolarization, scintillation, and dispersion effects. This is because, in principle at least, the loss of signal due to attenuation may be recovered by using a more powerful source or a more sensitive receiver. The latter effects, however, have to do with the "randomizing" of the signal, and hence, cannot be recovered likewise. Therefore the meaningful measure of the performance of the EM wave transmission should be a signal-to-noise ratio rather than simply an attenuation ratio.

The other dimension of the atmospheric effect is that the property of the medium is a function of time. For short time fluctuations (of a time scale of the order of the unit message length), the overall effect is equivalent to a noise component. Over a long time, however, there may be occurrence of severe events such as thunderstorms during which the communication link may be lost for a period of time. These factors have to

be considered in the reliability of the transmission system. (See Section 6.)

4.1 Attenuation Due to Gaseous Absorption

The attenuation of EM waves by absorption by atmospheric gases is unavoidable, and transmission wavelengths have to be chosen in the clear windows of the absorption spectrum. The main absorbing gases in the atmosphere are water vapor, carbon dioxide, ozone, and oxygen. In addition, minor species such as carbon monoxide, methane, and oxides of nitrogen also absorb radiation. Water vapor and ozone, being asymmetric top molecules, have rich electronic, vibrational and rotational spectra. The absorption in the ultraviolet is mainly due to oxygen and ozone. The visible region is, by and large, clear. The infrared region is dominated by the vibrational rotational bands of water vapor and carbon dioxide. In the microwave and submillimeter wave region, the significant absorbants are oxygen and water vapor (Figure 4-1). Detailed calculations of the absorption properties due to the atmospheric gases from spectroscopic constants and quantum mechanical models exist and are beyond the scope of this review. The calculations, however, are dependent on line width constants which are functions of the temperature, pressure and humidity of the atmosphere. All of these parameters vary with geographical locations, altitudes, season of the year and time of the day. Transmission models based on high resolution line-by-line

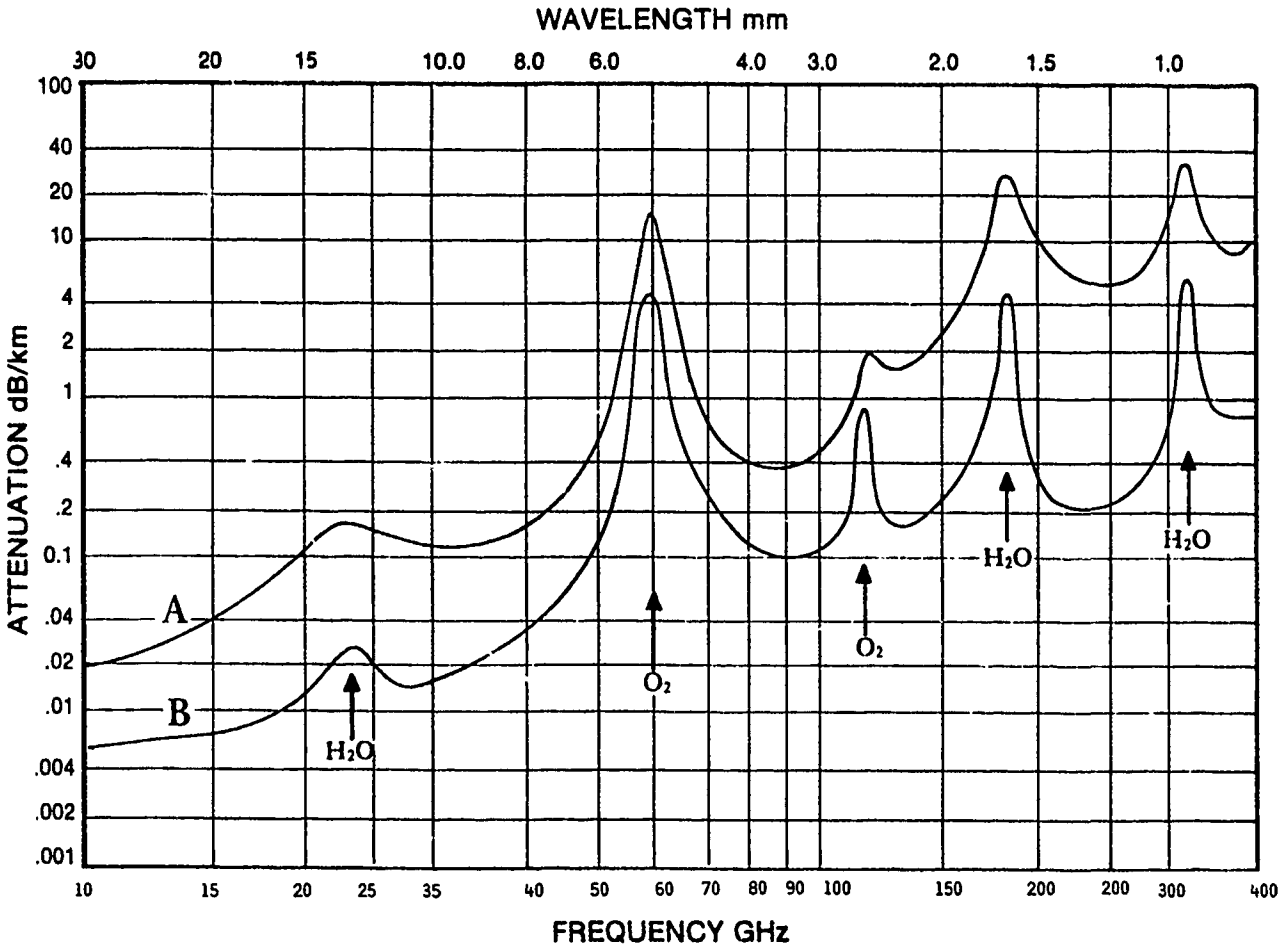

Figure 4-1. Clear-air attenuation of millimeter and centimeter waves from 3 cm to 0.8 mm. Curve A is for sea level ($T = 20°C$; water vapor density is 7.5 g/m^3). Curve B is for 4 km altitude ($T = 0°C$, water vapor density is 1 g/m^3). (Ref. 8)

calculation models or band models exist and are readily available in the literature. (See, for example, Refs. 5, 6, and 9.)

4.2 Hydrometeors

Atmospheric particulates both absorb and scatter EM radiation. Both effects result in attenuation of the signal. The most common atmospheric particulates are the hydrometeors (rain, snow, cloud and fog) and other particulates (dust and smoke) occurring naturally or man-made. For this report, we only consider hydrometeors. These particles range from millimeter in size (raindrops and snowflakes) to the micrometer range (fog and cloud droplets), and are usually characterized by a droplet size distribution rather than a single size. The presence of hydrometeors depends on the weather conditions of the location, and can have geographical and seasonal variations. When they are present, however, they may seriously impede the normally clear atmospheric gaseous absorption windows. For example, attenuation by gaseous absorption in the visible region is of the order of 0.01 db/km, but in the presence of a dense fog, the attenuation may exceed 100 db/km. (This is discussed in more detail in Section 5.) Therefore, to design a reliable EM wave link, it is necessary to attend to the nature of the hydrometeors, both in terms of their effect on EM wave propagation, and in terms of the likelihood of their occurrence.

4.2.1 Attenuation Modelling

The attenuation of EM waves at wavelength λ by particles is characterized by the local extinction coefficient $k(\lambda,x)$ so that the total attenuation A(db) is given by

$$A(db) = 4.343 \int_0^L k(\lambda,x)dx \qquad (1)$$

where the integration path is along the line of sight. Except at wavelengths close to the resonant frequencies of the molecular constituent of the particles (regions of anomalous refractive index), the variation of k as a function of wavelength is normally not significant over the bandwidth of the transmission, so that the EM wave may be considered as monochromatic.

The extinction coefficient k may be calculated from basic principles if the properties of the particles are known. The expression for k may be written in a generic form as

$$k = \int d\phi \int_0^\infty dr\ r^2 Q_{ext}(r,m,\lambda,\phi)\ N(r,\phi,x,t) \qquad (2)$$

where Q_{ext} = extinction efficiency

r = particle size

m = refractive index = $n - in'$

n = real part of refractive index

n' = imaginary part of refractive index

λ = wavelength

ϕ = variable describing the composition of the particle

N = size distribution

x = position

t = time

The integrations are over all the different particle compositions ϕ and sizes r. The extinction (i.e., total attenuation) efficiency Q_{ext} consists of a scattering part and an absorption part

$$Q_{ext} = Q_{scat} + Q_{abs} \tag{3}$$

The scattering part is due to the interference effect of the induced dipole radiation with the incoming radiation. The absorption part is due to the dissipation of the radiation in the particles and is mainly governed by the imaginary part of the refractive index. The calculations of Q_{scat} and Q_{abs} are governed by the classical electromagnetic theory (Ref. 7). These calculations, known as Mie theory, consider the case of a dielectric sphere in the radiation field, and obtain the solution for the Maxwell's equations with the appropriate boundary conditions at the surface of the sphere. The important parameter in the calculation is not the wavelength λ nor the particle radius r, but the non-dimensional ratio a:

$$a = 2\pi r/\lambda \tag{4}$$

For particles small compared to the wavelength ($a \ll 1$), for example, for microwave propagation through clouds, the Mie theory reduces to the Rayleigh limit,

$$Q_{scat} = (8a^4/3)\mathrm{Re}\,[(m^2 - 1)/(m^2 + 2)] \tag{5}$$

$$Q_{abs} = -4a\ \mathrm{Im}[(m^2 - 1)/(m^2 + 2)] \tag{6}$$

Note that in this limit, the scattering part becomes very small because from Eqs. (2)-(5), the extinction coefficient due to scattering is proportional to r^6 because of the r^2Q_{ext} term.

For particles large compared to the wavelength, for example, for the transmission of visible light through raindrops, the extinction coefficient reaches an asymptote.

$$Q_{ext} = 2 \tag{7}$$

This result may be obtained from considering the $a \gg 1$ limit of Mie theory or from Babinet's principle (Ref. 7). The latter is more general because it is valid independent of the shape or the optical properties of the particle.

It should be noted that in Eq. (2), the particle size is characterized by a radius r. In general, the particles are not spherical. From a practical standpoint, an effective radius is used, notwithstanding that this effective radius is actually dependent on the experimental method in measuring it. For example, the same particle may have a different optical radius

than an aerodynamic radius. Furthermore, the composition ϕ of the particle (such as the mass fraction of ice in a freezing rain, for example) is usually not well known. In spite of these limitations, predictive calculations employing the Mie theory on spherical particles with uniform composition are often used to obtain estimates of the effects.

The other factor in the calculation of the attenuation (Eq. (2)) is the particle size distribution $N(r, \phi, x, t)$ defined as the number of particles with size in the range $(r, r + dr)$ and composition range $(\phi, \phi + d\phi)$. The total droplet density would be obtained by summing over all the sizes and the categories of composition

$$N_{total}(x,t) = \int d\phi \int_0^\infty dr\, N(r, \phi, x, t) \qquad (8)$$

The space and time dependence of N should be noted. For example in a typical cloud, the value of N_{total}, the shape of the size distribution, and the ice/water composition are all a function of the altitude and time. Experimental data on the typical size distributions of the different types of hydrometeors (rain, cloud, fog and snow) exist, and are often given in various curve fitted functional forms. Information on the composition is less available. However, the AFGL/CSU model can estimate this composition.

The foregoing discussion points to the critical information needed to evaluate the attenuation due to the

hydrometeors. The discussion may be summarized by examining the terms in Eqs. (1) and (2), which require knowledge of the complex refractive index, the composition, and the size distribution of the particles. The latter two are both a function of space and time, so that the total contribution to attenuation needs to be integrated along a line of sight, and the effects need to be examined over time.

4.2.2 Optical Constants

Figures 4-2 and 4-3 show the complex refractive index of water and ice (Ref. 10), respectively from 1 μm to 100 m. Figure 4-4 shows the refractive index of water and ice from 0.2 μm to 100 μm (Refs. 11 and 12). Figure 4-5 shows the refractive index of ice from 0.05 μm to 10 m (Ref. 13). In Figures 4-3 and 4-5, it is shown that the imaginary part of the refractive index in the MMW and microwave regions is very sensitive to the ice temperature. There is less variation with temperature for water. (See Refs. 9 and 10.)

4.2.3 Size Distribution

Since each class of hydrometeors consists of a range of particle sizes, it is necessary to distribute the mass loading of the aerosols and airborne particles to a size distribution for

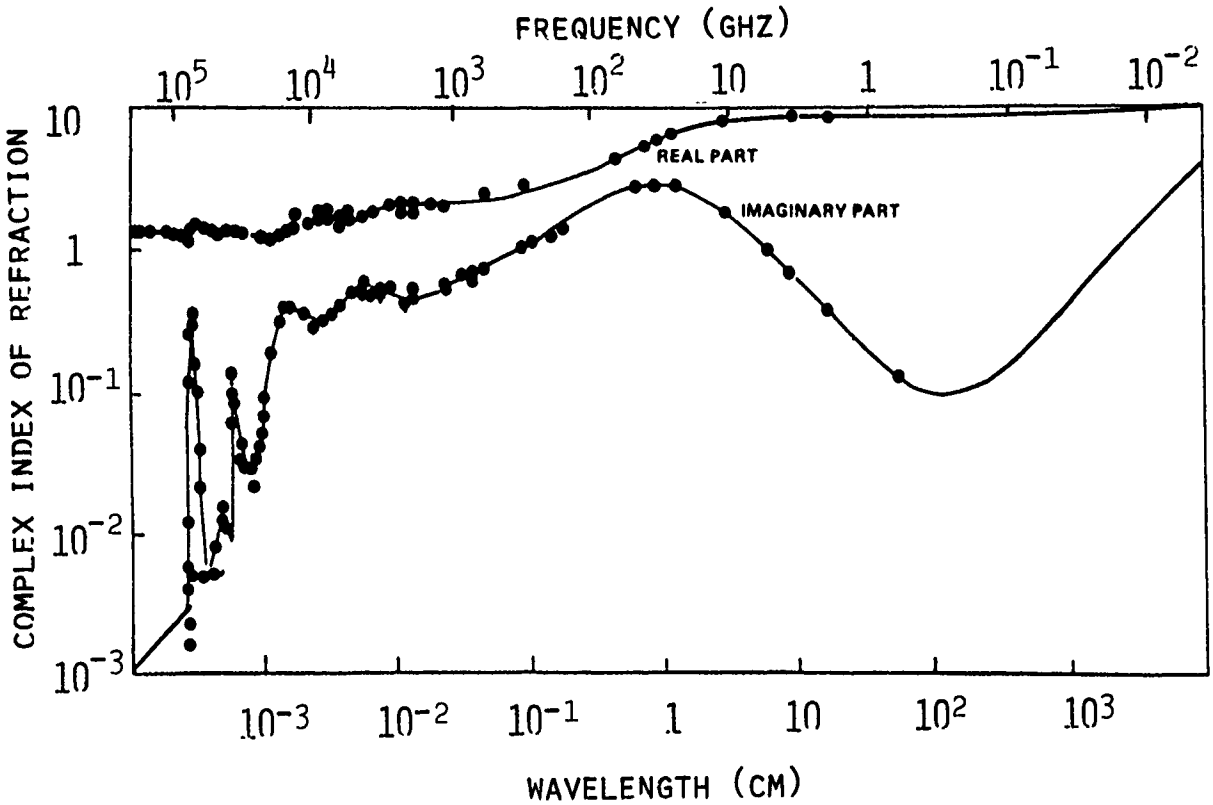

Figure 4-2. Complex Refractive Index of Water (Adapted from Ref.10)

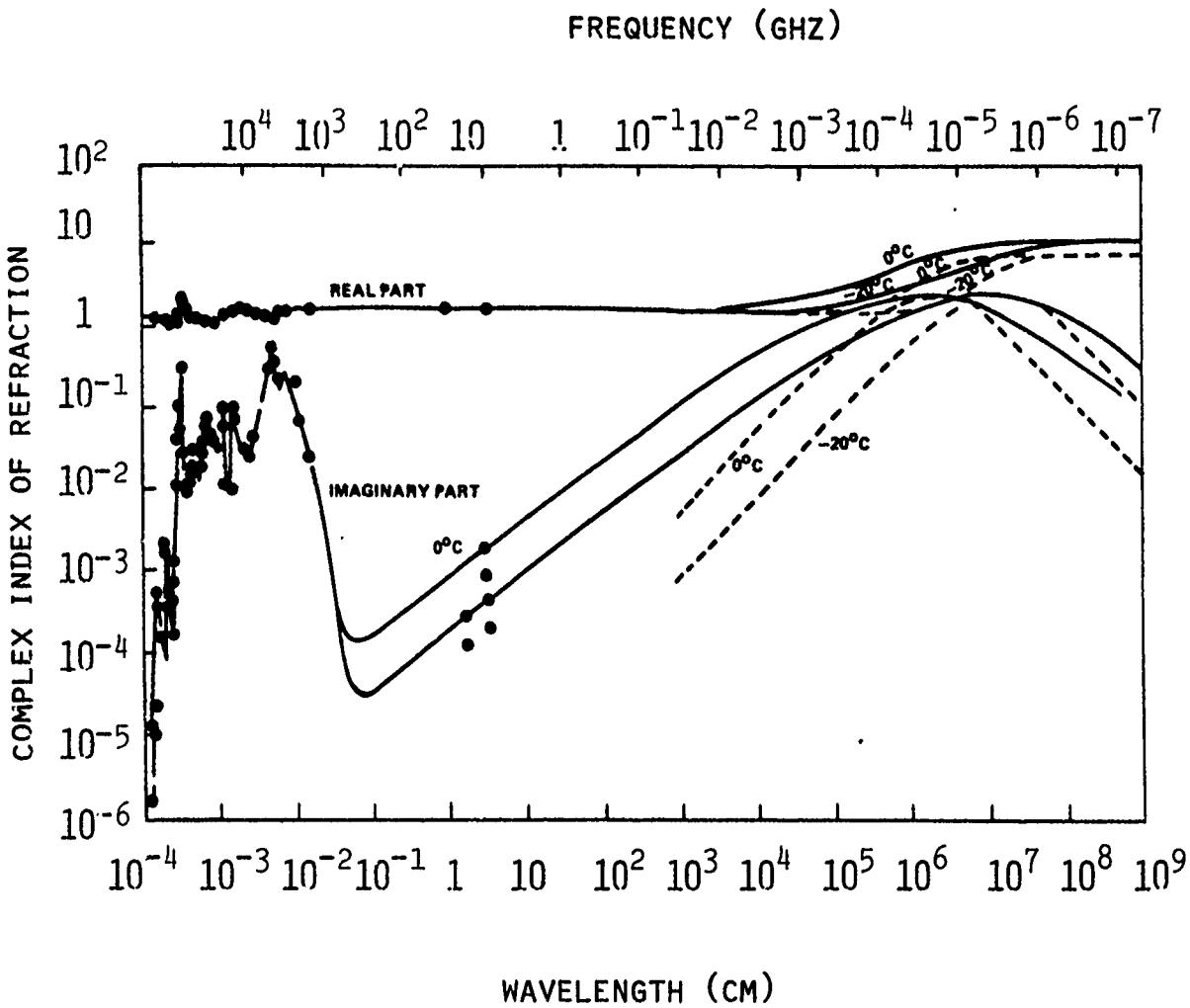

Figure 4-3. Complex refractive index of ice (Adapted from Ref. 10).

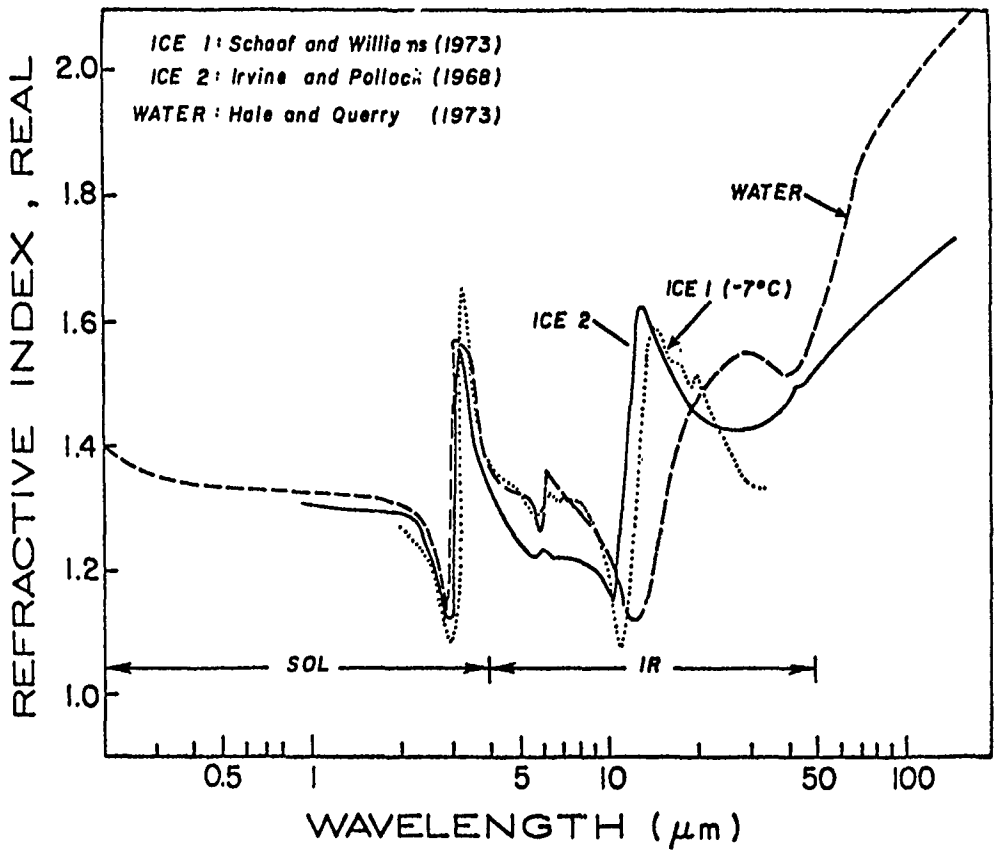

Figure 4-4. Real Part of the Refractive Index for Ice and Water as a Function of Wavelength. (Adapted from Refs. 11 and 12.)

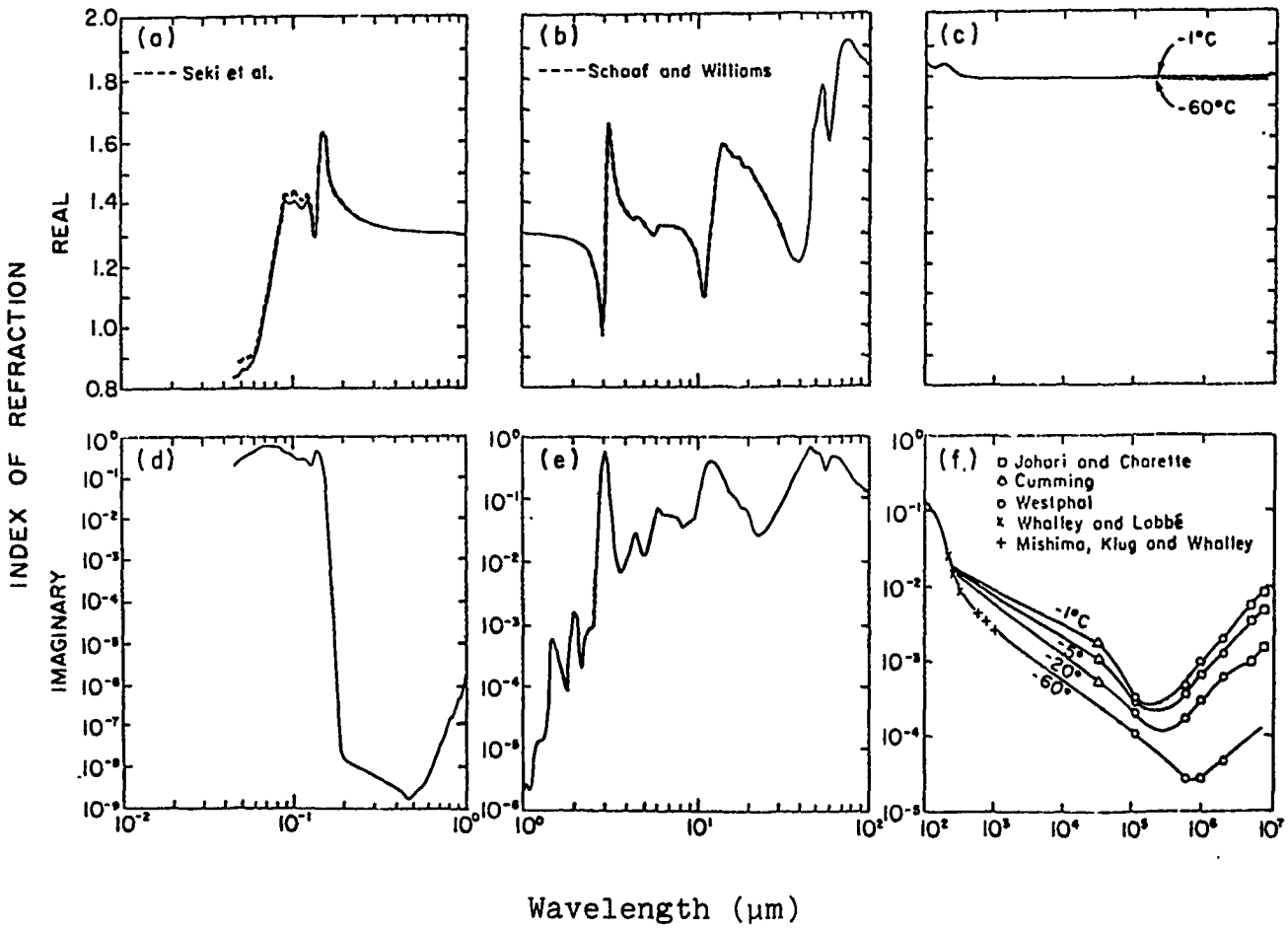

Figure 4-5. Refractive Index of Ice (0.05 μm to 10 m) (Ref. 13)

attenuation calculations. Figure 4-6 shows representative size distributions for several types of liquid water aerosols (Ref. 14). Various forms of curve fits may be applied to these distributions. The more popular ones are in terms of log-normal distribution, power law, combination of powers and exponentials and the gamma distribution (Refs. 15, 16, 17). The AFGL/CSU model uses a Marshall Palmer distribution (Ref. 15) with a constant slope for the rain drop size distribution (see Figure 4-7). Both the Marshall Palmer (Ref. 15) and the Joss (Ref. 17) distributions are written in the form of

$$N(r) = N_o \exp[-A(R)r] \qquad (9)$$

where R is the rain rate in mm per hour and r is the drop radius in mm. N_o and A are empirically determined, with values shown below.

Distribution:	$N_o(mm^{-1}m^{-3})$	$A(mm^{-1})$
Marshall-Palmer	8×10^3	$8.2\ R^{-0.21}$
Joss: Drizzle	30×10^3	$11.4\ R^{-0.21}$
Widespread Rain	7×10^3	$8.2\ R^{-0.21}$
Thunderstorm	1.4×10^3	$6.0\ R^{-0.21}$

The distribution for the cloud droplets that we recommend is a one-parameter gamma distribution (Ref. 18). The distribution function is:

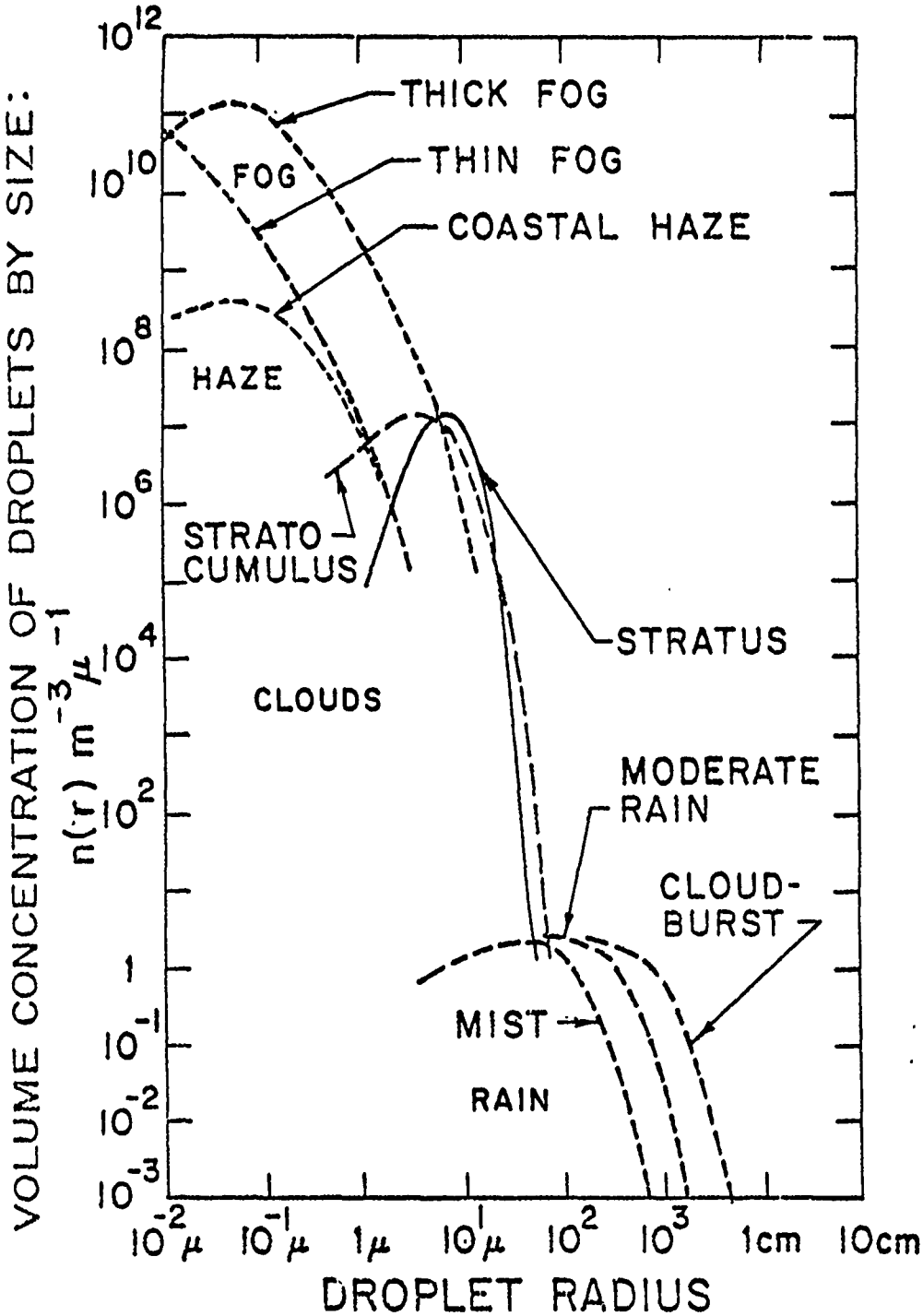

Figure 4-6. Example of water aerosol distribution functions. (Ref. 14)

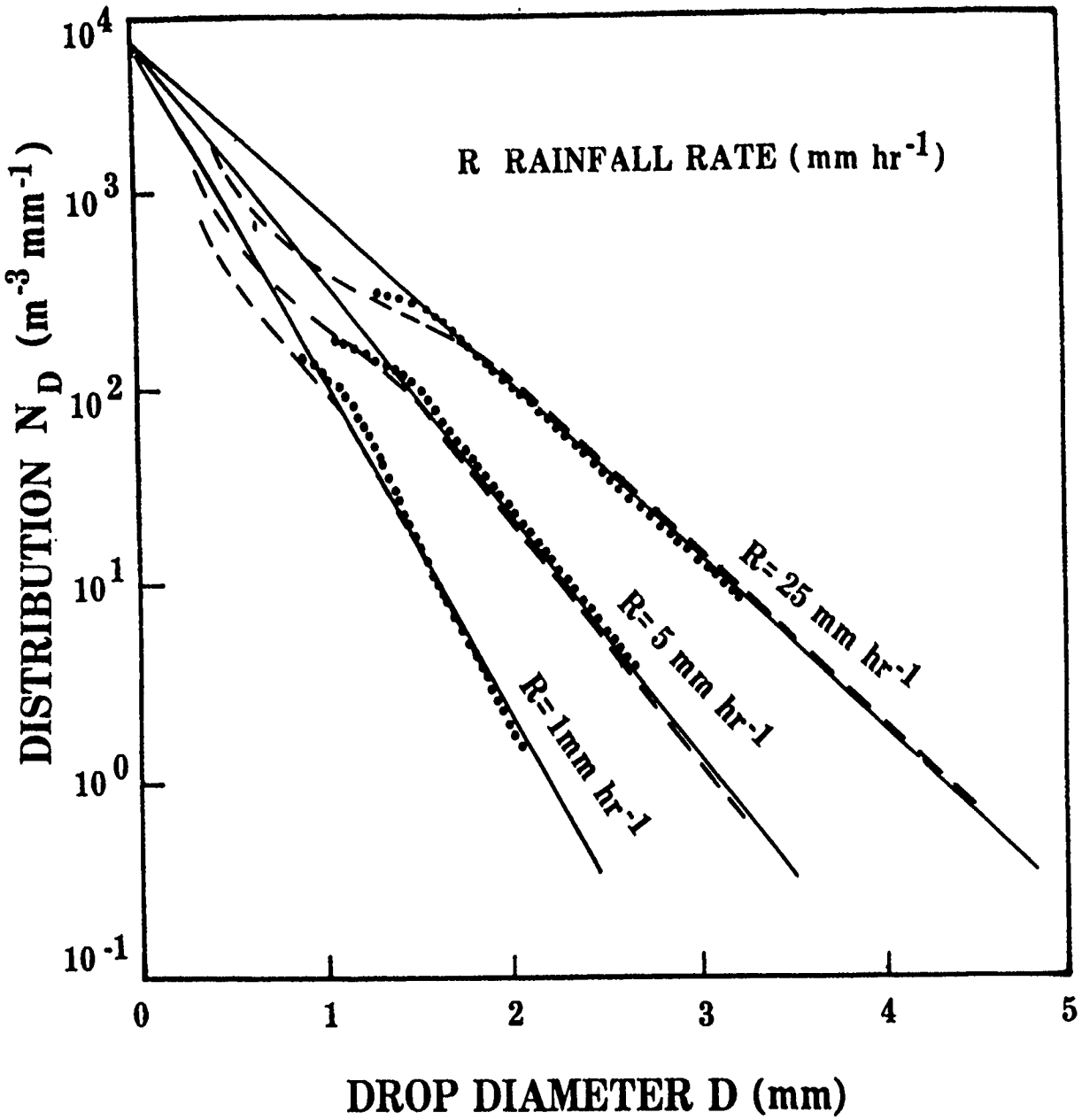

Figure 4-7. Laws-Parsons (dashed line) and Marshall-Palmer (dotted line) distribution of raindrops. (Refs. 15, 16)

$$N(r) = Ar^2 \exp(-Br)$$

where

r = droplet radius in cm

$A = 1.45 \times 10^{-6} (w/\rho)(\bar{r})^{-6}$

$B = 3/\bar{r}$

w = liquid water content in g/m^3

ρ = density of water in g/cm^3

$\bar{r}$ = mean radius in cm

Alternatively, a cloud droplet size distribution depicted in Figure 4-8 can be used (Ref. 19).

The description of hydrometeors in the ice phase is more difficult. The ice crystal shape is related to the conditions of formation. A single crystal or polycrystal may form; the shape depends on the growth environment and may lead to hexagonal plates or dendrites, hexagonal pencil-like columns, or an open structure in the form of irregular needles or dendrites. To simplify the description, an equivalent diameter which loosely describes the size is often used. A typical size distribution of ice crystals in the atmosphere is shown in Figure 4-9 (Ref. 20). Figures 4-10 and 4-11 and Table 4-1 provide distributions found by various researchers for different ice particle types (Refs. 21, 22).

The interaction of irregular ice particles with an electromagnetic wave is a complex one. Fortunately these particles are randomly oriented in space, and, on the average, may be treated by using Mie theory on an ice "spherical" particle of an equivalent diameter, notwithstanding that the

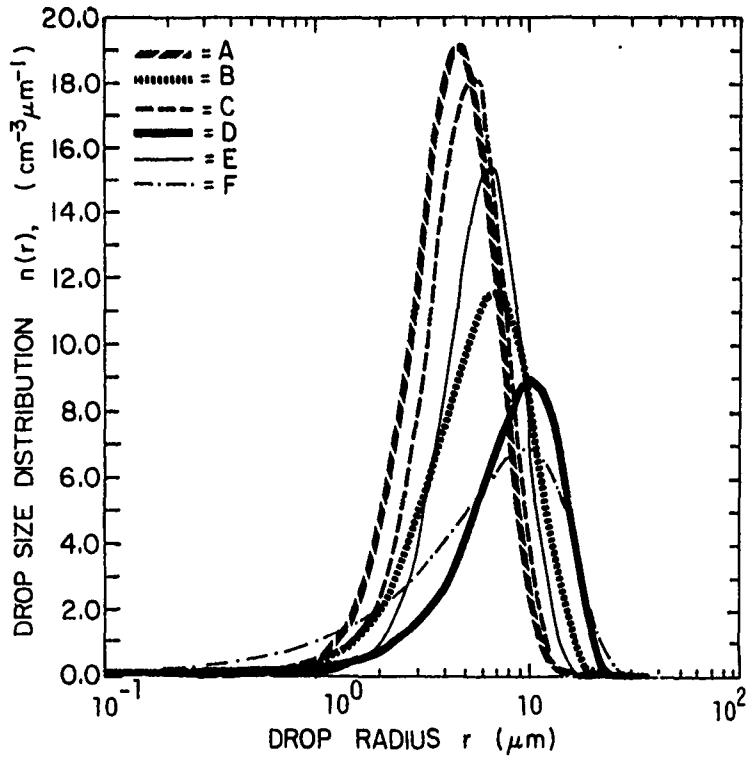

Figure 4- 8. Drop size distributions n(r) for various cloud cases: A) stratus base; B) stratus top; C) stratocumulus base; D) stratocumulus top; E)nimbostratus base; F) nimbostratus top. (Ref. 19)

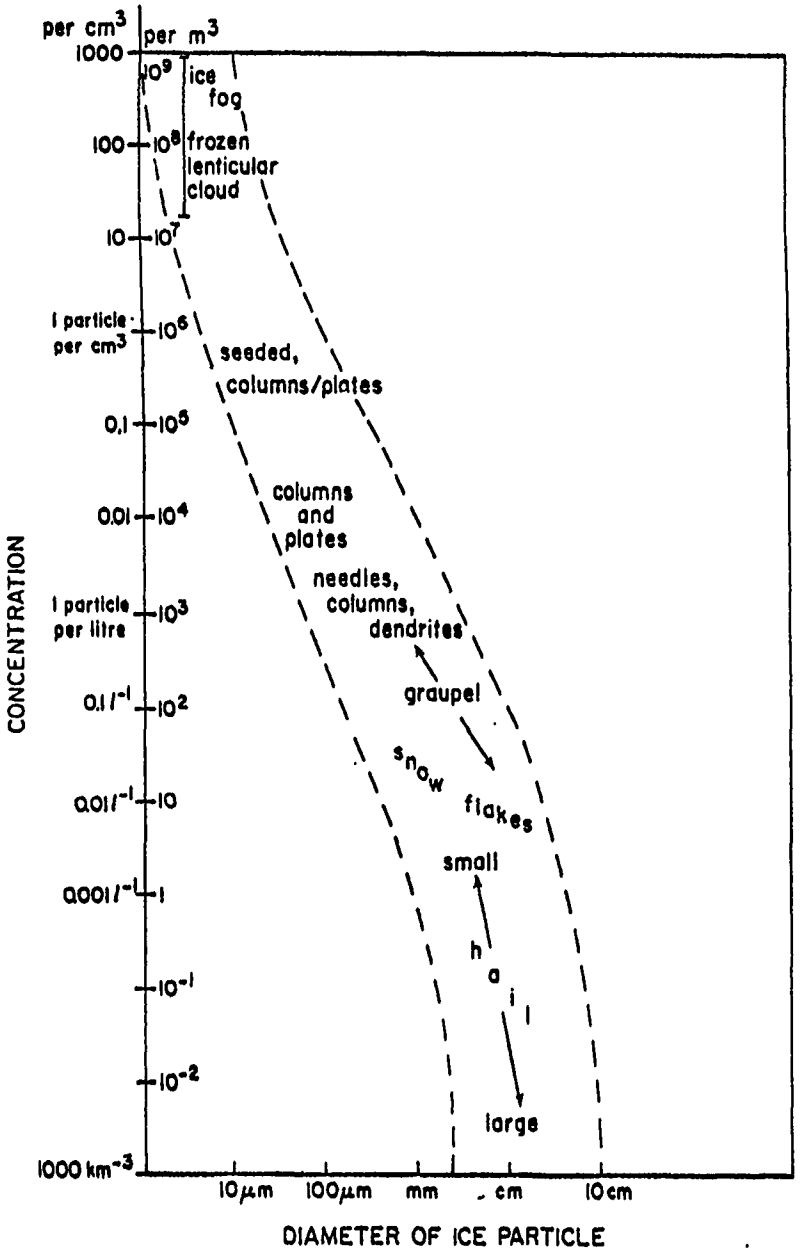

Figure 4-9. Typical size, concentration and variance of ice particles in the atmosphere. (From Hallett, Ref. 20)

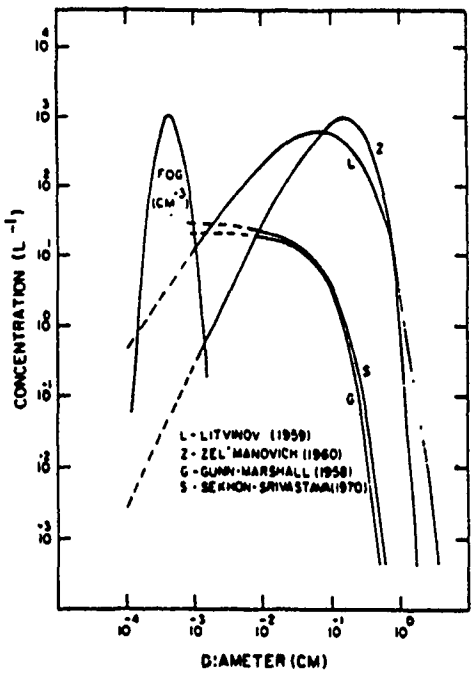

Figure 4-10. Particle size distributions for falling aggregates of snow crystals. (Ref. 21.)

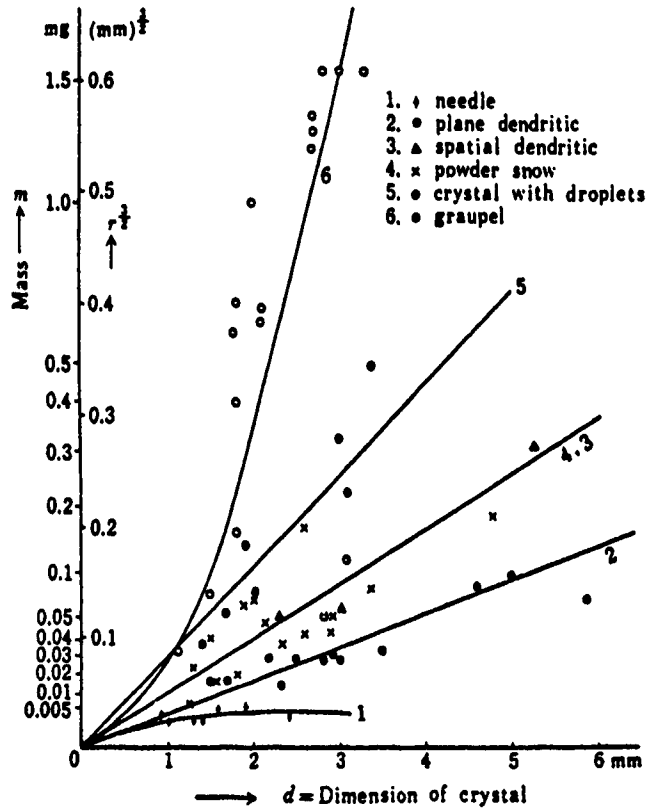

Figure 4-11. Mass and dimension of various ice crystals. (Ref. 22)

Table 4-1. Approximate relationships between snowflake crystal mass and dimension (Ref. 22)

Snow Type	Correlation*	Proportionality
Graupel**	$m = 0.065d^3$	To Volume
Crystals with Water Droplets	$m = 0.027d^2$	To Surface Area
Powder Snow and Spatial Dendritic Crystals**	$m = 0.010d^2$	To Surface Area
Plane Dendritic Crystals**	$m = 0.0038d^2$	To Surface Area
Needles	$m = 0.0029d$	To Length

*m = mass (mg); d = dimension (mm)

**Average thickness ≈ 0.011 ± 0.002 mm

precise relationship between the equivalent diameter and the actual ice crystal size and shape is unknown. We recommend fitting power law relationships to the various ice particle distributions, i.e., fitting straight lines to the different segments of Figure 4-9.

The above hydrometeor distributions are averages over many sets of data. For any single situation, there may be significant departures from these mean distributions, and care must be taken when interpreting data because of this. This presents limitations to using these distributions for calculation of attenuation in a specified real-time case. On the average, however, these distributions can be used when looking at average propagation properties.

5. OVERALL ATTENUATION RESULTS

A number of field tests and various calculations using Mie theory have been carried out for the attenuation of EM waves over the microwave to the UV spectrum. Some of these results (Refs. 23-25) are summarized in Figure 5-1 with further details given in Figures 5-2 to 5-5. (The attenuation due to clouds is not shown in Figure 5-1 but is shown in Figure 5-4.)

The parametric set of curves in Figure 5-3 were calculated for attenuation due to rain. As can be seen, there is a substantial increase in attenuation as the frequency increases from 10 GHz up to 300 GHz, with a peak around 100 GHz. Figure 5-5 shows UV, visible, IR, and MMW attenuation due to falling snow. These results are based on our analysis of measurements made at the SNOW field test exercises conducted by the U. S. Army Cold Regions Research & Engineering Laboratory. As indicated in Figure 5-5, attenuation due to falling snow will be significant at some frequencies if the path length is several kilometers.

The various trade offs in designing a communication band are obvious from Figure 5-1. While the visible region is almost transparent in clear air, the attenuation is substantial in the presence of hydrometeors, and is almost opaque in dense fog. The same can be said for the gaseous transmission windows in the infrared region (1-30 μm). The far infrared and the short submillimeter wave are dominated by the strong absorption bands of the water vapor. However in the millimeter wave and microwave regions, there are clear windows for transmission.

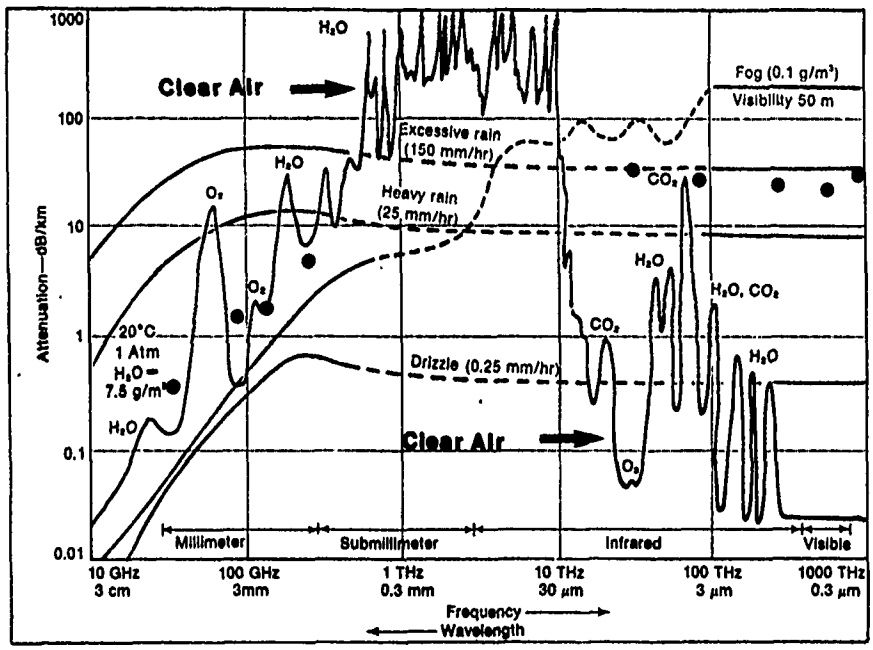

Figure 5-1. Atmospheric transmission at sea level for wavelengths 3 cm to 0.3 μm. (Ref. 23) The symbols (●) indicate attenuation for moderate snowfall using our analysis results shown in Figure 5-5.

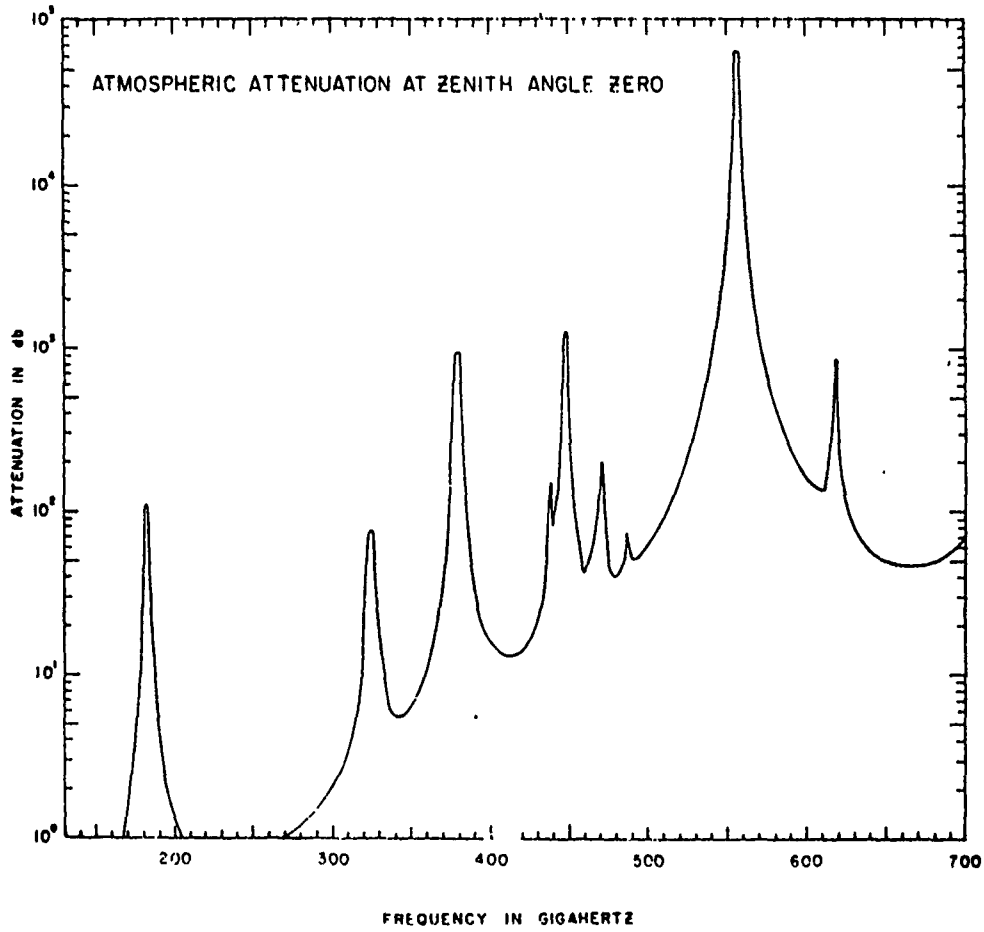

Figure 5-2. Total clear air zenith attenuation from sea level ($T = 27^{\circ}C$; water vapor density = 7.5 g/m^3). (Adapted from Ref. 24)

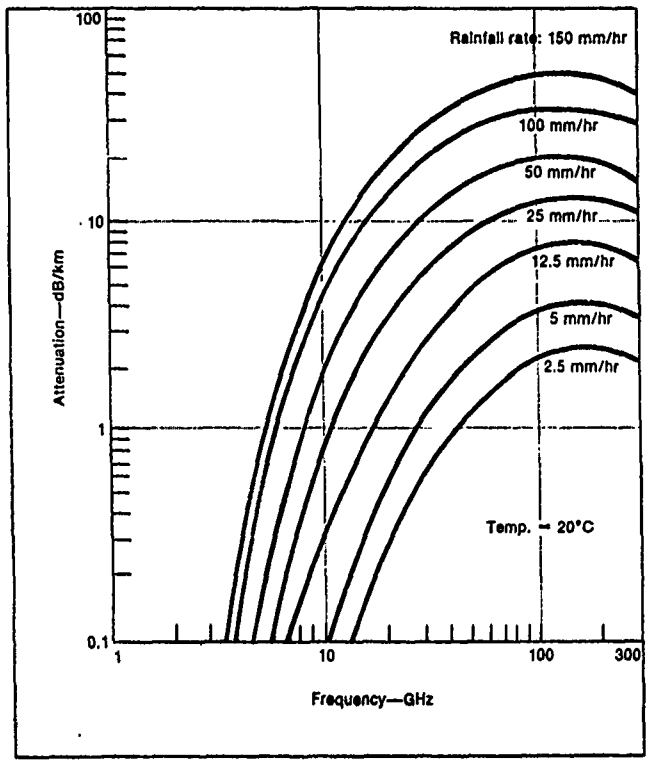

Figure 5-3. Attenuation due to rain. (Ref. 23)

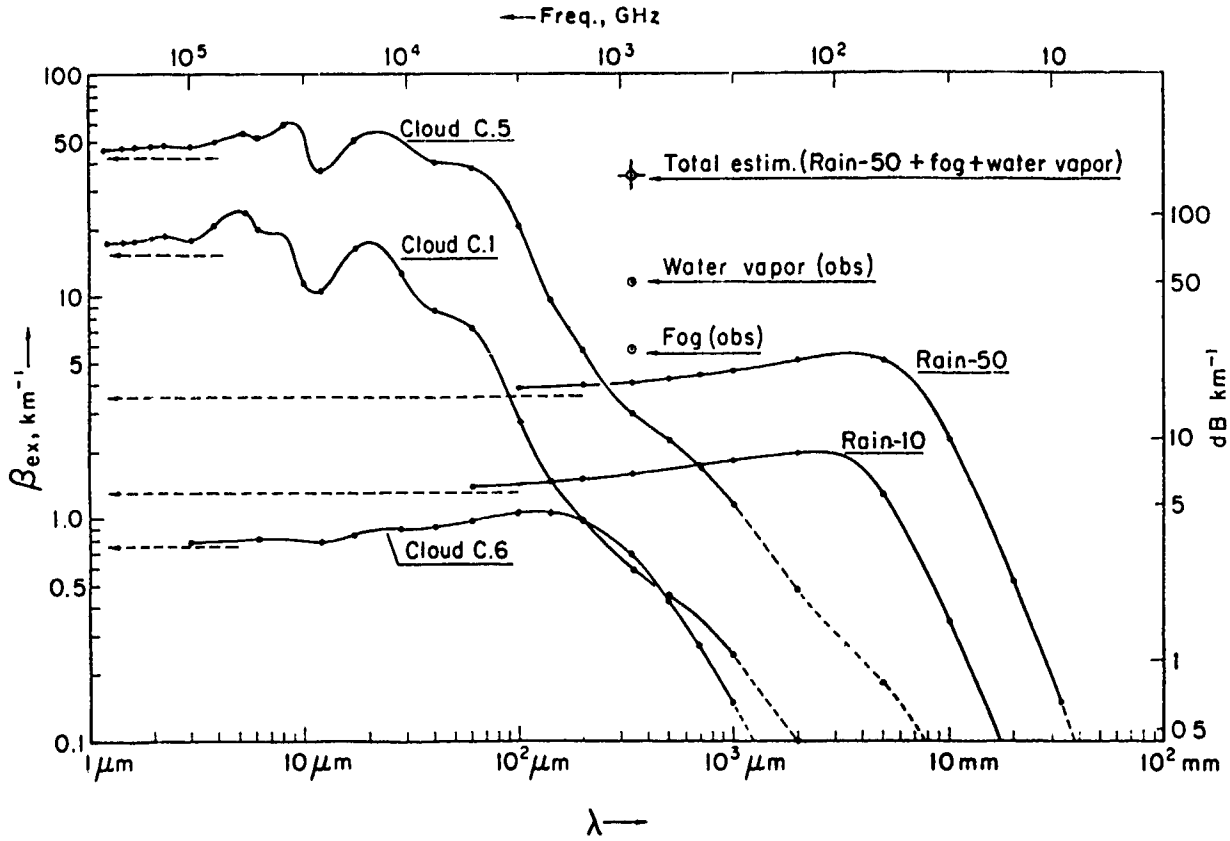

Figure 5-4. Theoretical Extinction Coefficients According to Three Cloud Models and Two Precipitation Models. Cloud model C.1, C.5, and C.6 are representative of cumulus clouds, nimbostratus, and large-droplet nimbostratus, respectively (Ref. 25).

ATTENUATION IN SNOWFALL

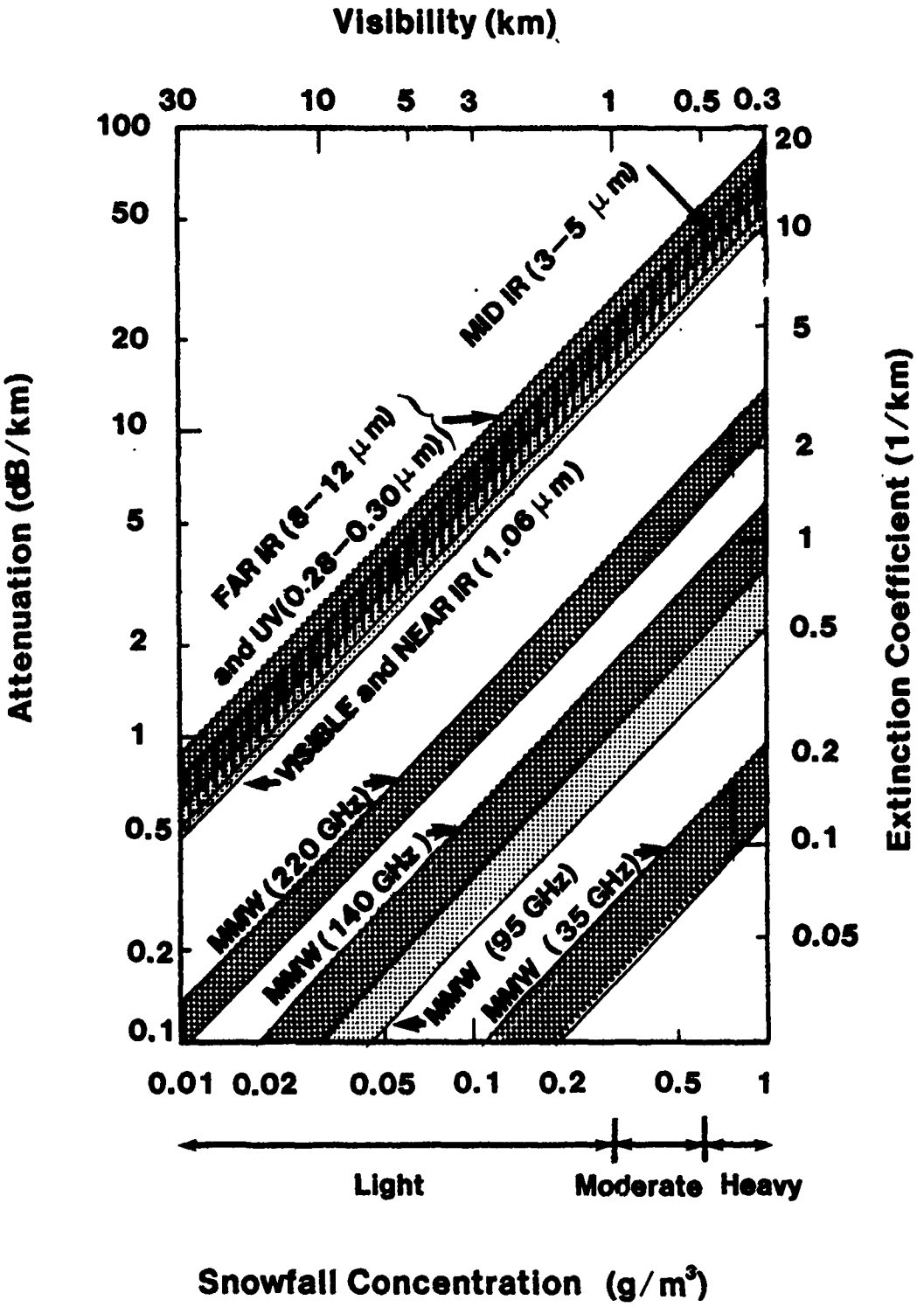

Figure 5-5. Attenuation due to falling snow for UV, visible, IR and MMW based on our analysis of measurements made at the SNOW field tests.

Furthermore, the attenuation of MMW and microwaves in these regions due to fog and clouds is small because the wavelength is large compared to the particle sizes (Rayleigh regime). Therefore these regions will be attractive as communication channels. However, depolarization effects due to ice crystals in the cloud may be important and are discussed in Section 6.

Backscatter of active MMW and microwave radar systems is an important phenomenon related to attenuation. This is indicated in Figure 5-6 for rain over the frequency range 10 to 1000 GHz. As can be seen, there is a peak at approximately 40 GHz which shifts to about 200 GHz as the rainfall rate decreases. Thus, a substantial backscatter problem can occur for MMW and microwave signals.

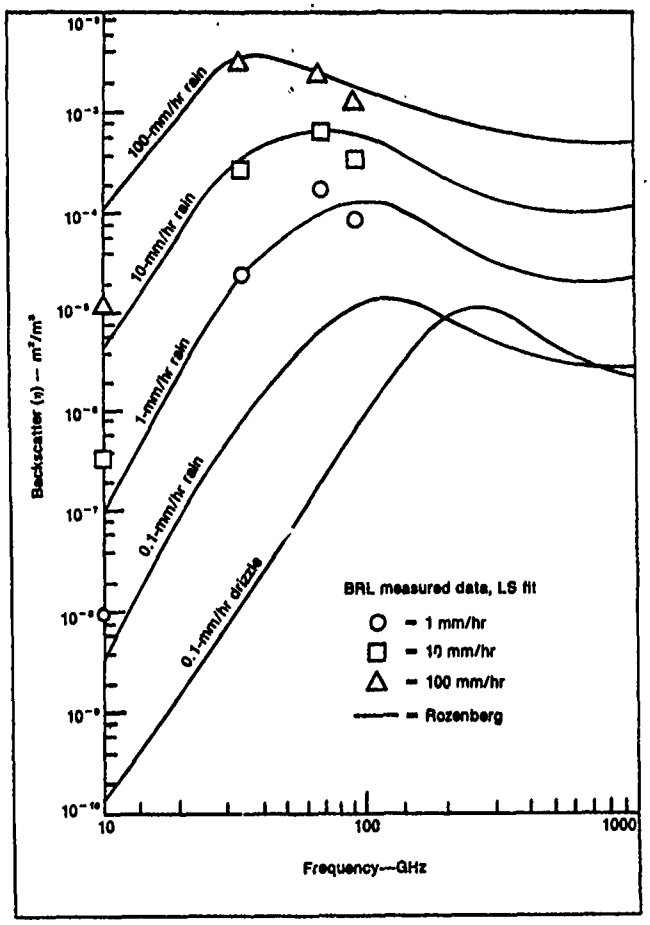

Figure 5-6. Backscatter due to rain. (Ref. 23)

6. MILLIMETER WAVE AND MICROWAVE PROPAGATION

As was seen from Figures 4-1 and 5-1, there are atmospheric windows near frequencies of 35 GHz, 95 GHz, and 140 GHz. At the very low end (10 GHz), there is very little atmospheric attenuation. Microwave links (frequency lower than 30 GHz) have been used for some time with reasonable cost and high reliability. There is, however, a need for constant improvement of these systems. For example, the reliable but overcrowded microwave bands no longer have sufficient channel capacity to accommodate the projected explosive increase of information transfer in digital communications. Thus the technology is being pushed towards the MMW wave (EHF) arena. In addition, the communications must be robust, i.e., all-weather and low-error-rate. Therefore the effects of hydrometeors on MMW propagation need to be addressed.

It was evident from Figure 5-1 that while the attenuation is low for clear air at the atmospheric windows of MMW, there is a considerable amount of attenuation when there is rainfall. This is due primarily to a large absorption coefficient resulting from a large imaginary part of the complex refractive index of water, as was indicated in Figure 4-2. Comparing this to Figure 4-3, the complex refractive index for ice, it can be seen that at near 1 mm wavelength, the imaginary part of the index is substantially larger for water than for ice. In ice the molecular dipoles commonly respond to frequency $\gtrsim$ 10 KHz, since the dipole rotation rate is defect controlled; in the

liquid the dipoles rotate as individuals with a frequency ≈ 10 GHz which is equivalent to wavelengths of ≈3 cm, hence the difference.

The attenuation of an EM wave by water or ice can be calculated in principle by Mie theory when the hydrometeors are comparable in size to the wavelength of interest, by Rayleigh theory when the hydrometeors are small, and by geometrical optics for large particles (Ref. 7). For MMW and microwave frequencies, either Mie or Rayleigh theory will be applicable. However, as reviewed in Section 4, the uncertainty of attenuation prediction lies not in the application of EM wave theory but in the limited amount of information available on the nature of the hydrometeors: their composition, size distribution as well as the spatial and temporal distributions.

Besides attenuation, there are other issues which are pertinent to the effects of hydrometeors on EM wave propagation. These are depolarization, scintillation and bandwidth coherence. Furthermore, there is also the occurrence of periods of severe weather conditions such as thunderstorms which may cause a blackout, and means to evaluate the reliability of the system have to be examined. These topics are discussed below.

6.1 Depolarization

To double the channel capacity of the communication link, the two orthogonal (or left- and right-circular) polarization channels are used. Rain induces depolarization (cross-polarization) because of the differential attenuation and phase shift caused by the non-spherical raindrops (Ref. 4). When the raindrops are small, the surface tension force is dominant and the droplets are spherical. As the droplets grow in size by condensation and agglomeration, the gravitational force and the aerodynamic drag force take over, and the droplets take the shape of an increasingly flattened oblate spheroid, or even with a concave base (Ref. 26). There is also evidence that the shape oscilates. Furthermore, the deformed spheroids may be canted to the horizontal because of the presence of vertical wind shear. (Although the mean wind shear is not strong enough to accomplish this, local wind shears associated with turbulent mixing can give rise to this on a scale of meters.) The depolarization nature of a canted oblate spheroidal drop is illustrated in Figure 6-1. The result of the depolarization is a cross-talk between the two normally orthogonal polarization channels.

To evaluate the depolarization effect, a cross-polarization descrimination (XPD) factor may be used. Referring to Figure 6-1, for a linearly polarized wave, the XPD is defined by (Ref. 4):

$$XPD = 20 \log (|E_{11}|/|E_{12}|) \qquad (10)$$

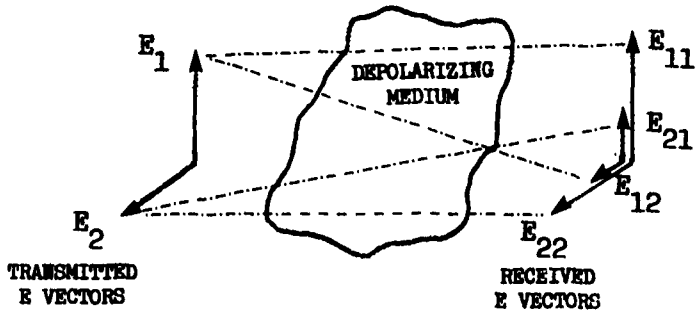

E_{11} E_{22} - CO POLARIZED WAVES

E_{12} E_{21} - CROSS POLARIZED WAVES

(a)

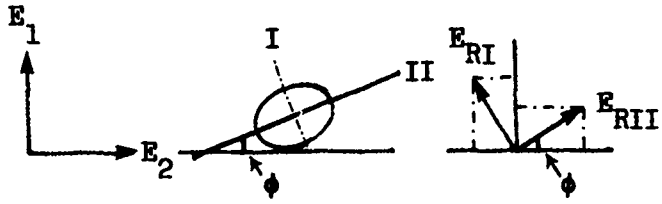

CANTED
OBLATE SPHEROIDAL
DROP
(b)

Figure 6-1. Vector relationships for a depolarizing medium (a) co- and cross-polarized waves for linear transmission, and (b) classical model for a canted oblate spherical raindrop (Ref. 4).

where E_{11} is the desired copolarized electric field and E_{12} is the undesired orthogonal cross-polarized field. A similar definition may be used for the circularly polarized wave. It has been found empirically, and justified on a theoretical basis (using small argument approximations) (Ref. 27), that the rain-caused XPD and the attenuation are correlated. A typical cross plot is shown in Figure 6-2 taken from Ref. 28. The empirical correlation is in the form of

$$XPD = U - V \log (A) \qquad (11)$$

where U and V are empirically determined functions of frequency, polarization, elevation angle, canting angle, and other link parameters.

The depolarization effects due to the ice crystals above the melting layer is less well known. It has been referred to as the "anomalous" depolarization. It has been observed in satellite-to-earth links (Refs. 29, 30). This depolarization effect does not correlate with attenuation. Because of the low imaginary part of the refractive index of ice, the depolarization is mainly due to the phase shift. The data from the satellite-to-earth link at 11.7 GHz experiment (Ref. 30) indicated that the anomalous depolarization due to the ice crystal is only significant at high XPD. This happens when the cross-polarization due to rain is small (i.e., the rain contributes only on the order of -3 db to the XPD).

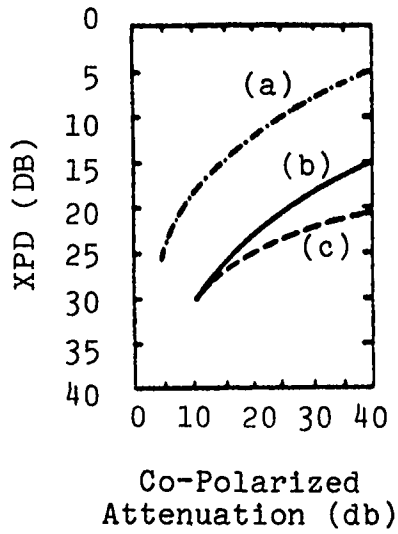

Figure 6-2. Cross-polarization discrimination (XPD) versus co-polarized attenuation warm rain (11 GHz) for the following transmitted waves: (a) circular, (b) linear horizontal, and (c) linear vertical polarization (Ref. 28).

6.2 Scintillation

Scintillation describes the rapid fluctuations in amplitude, phase and angle of arrival of the signal due to the propagation through a medium with small scale irregularities in the refractive index. To a first approximation, the atmosphere may be considered as a vertically stratified layered structure. Turbulence at the interfaces of these layers gives rise to scintillation. As a result, scintillation is more pronounced for slant paths at low elevation angle. For satellite-to-earth links, the troposphere and ionosphere also contribute to the scintillation. In the troposphere, scintillation is caused by the humidity gradient and the temperature inversion layers at the first few kilometers. These scintillation phenomena are highly seasonal and vary from day to day.

A typical trace of the scintillation observed on the satellite-to-earth link using the ATS-6 satellite (Ref. 31) is shown in Figure 6-3 (a). The fluctuation for high elevation angles (20° to 30°) is of the order of 1 db (peak to peak) for clear sky in summer, and 0.2 to 0.3 db in winter. For cloud cover, however, the value may be up to 2 to 6 db. The frequency associated with the scintillation effect is of the order of 0.5 to 10 Hz. The elevation angle dependence is shown in Figure 6-3(b), in which the amplitude variance σ is fitted to a power law of the cosecant of the elevation angle

$$\sigma^2 = A(\text{cosec}\ \theta)^B$$

with $B \simeq 1.8$.

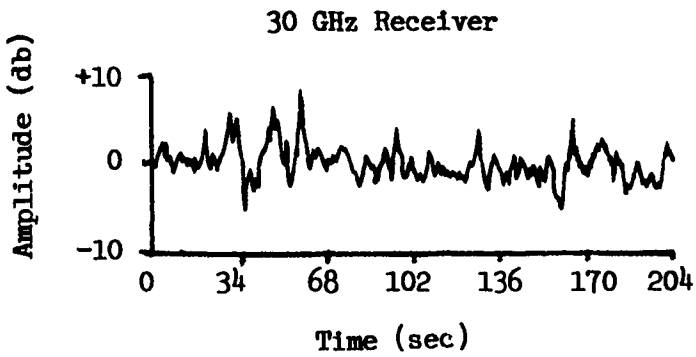

Figure 6-3 (a). Typical scintillation signal (Elevation angle: 4.95°)(Ref. 4).

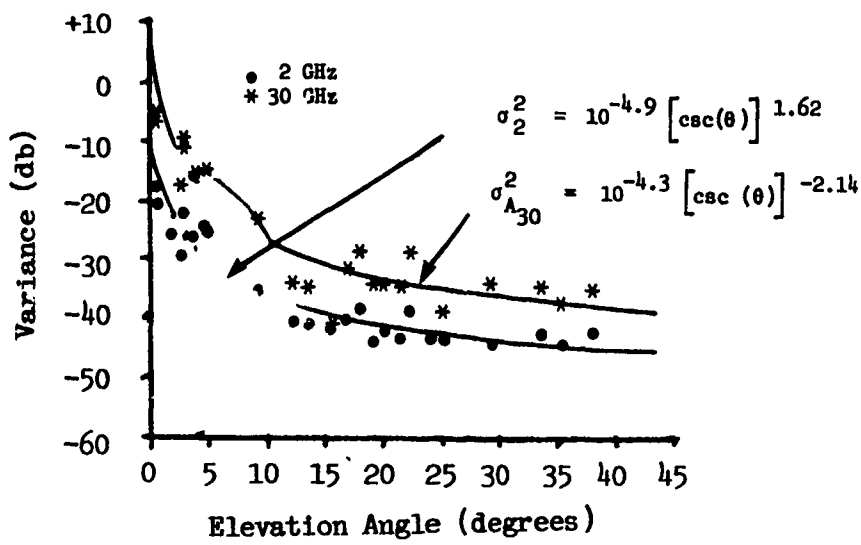

Figure 6-3 (b). Mean amplitude variance (Ref. 4).

6.3 Bandwidth Coherence

The discussion so far has been centered on the atmospheric effects on a monochromatic EM wave. For high speed communication, however, the effect on bandwidth needs to be considered. The loss of bandwidth coherence is mainly due to the phase and amplitude dispersions of the intervening medium. Experimental data have been reported with the ATS (Ref. 32) and the COMSTAR (Ref. 33) satellites for extensive periods. The conclusion of these studies was that "amplitude and phase dispersion should not pose a problem for wideband (on the order of 1 GHz) earth-space communication systems operating at frequencies greater than 10 GHz with relatively large elevation angles (>15°) from earth terminals".

6.4 Rain Attenuation Statistics

From Figure 5-1 and the previous discussion, it is evident that rain is the major source of attenuation for MMW and microwaves operating at the atmospheric windows. The occurrence of heavy rain or thunderstorms may cause such a high attenuation that the link may be temporarily lost. To ensure reliability of the communication, sufficient power margin over the normal signal-to-noise margin must be built in the system for these extraordinary events. This margin, of course, comes with an increase in cost of the system; hence the rain

statistics of the atmosphere medium need to be examined to get the proper trade off between cost and link outage rate.

Extensive rainfall statistics have been accumulated for different geographical areas. These statistics may be used to construct the attenuation statistics using the means as described in Section 4. Actual attenuation statistics over an extended time at limited geograpical locations have been recorded. Typical statistical results, over a three-year period (1976-1979) are shown in Figure 6-4. The yearly statistics are shown as the cumulative probability distribution of attenuation. This curve may be used to design the power margin required. For example, for a one-hour-per-year link outage, a power margin of 13.5 db is required for the worst of the three-year period measured. A link with a one-hour-per-year outage is considered to be of good quality, similar to that specified in the national phone system.

Based on the weather station information, the power margins required for link reliability for the temperate continental U.S. regions are shown in Table 6-1. A power margin of 6-10 db can be achieved with a reasonable cost, but 10-15 db can be costly and difficult.

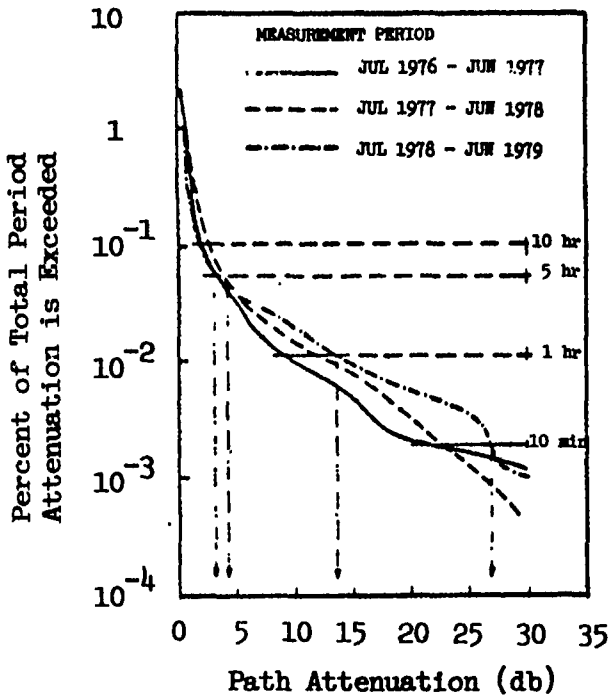

Figure 6-4. Probability distribution of attenuation measured at Greenbelt, MD. (Elevation angle: 29°; Antenna diameter: 4.5 m) (Ref. 4).

Table 6-1. Power margin for communication link reliability for temperate climate continental U. S. (Ref. 4).

Link Reliability (%)	Hours Per Year Outage	Power Margin dB		
		11 GHz	20 GHz	30 GHz
99.5	44	1	3	6
99.9	8.8	3	10	20
99.95	4.4	5	20	>30
99.99	0.88	15	>30	-

7. X-RAY PROPAGATION

7.1 Summary

X-rays are at the opposite end of the EM wave spectrum from microwaves. They are strongly attenuated by the atmosphere but may have space applications. Thus, we consider the absorption of X-rays propagating from space into the earth's upper atmosphere. For simplicity, this analysis considers a plane parallel atmosphere. However, the results can be readily modified to account for the earth's curvature. Absorption of the X-rays are parametrically computed for X-ray beams incident on the earth's atmosphere from 0° (directly downward vertical) to 60° slant path. Calculations are performed for an atmosphere with an exponentially decreasing density with altitude above the ground. The results show that X-rays propagating from space into the atmosphere will penetrate no further than an altitude of 120 km for 14 Å X-rays, and 60 km for 1 Å X-rays. These altitudes are well above those for clouds and precipitation. Hence, weather will have no effects on X-ray propagation from sources located in space.

7.2 X-Ray Propagation Issues

We consider the absorption of low energy X-rays propagating from space into the upper atmosphere.

Atmospheric absorption will be a serious problem at all X-ray wavelengths (Refs. 35, 40). Reports have been made of an X-ray laser developed at Lawrence Livermore Laboratory operating at a wavelength of 14 Å, corresponding to

a photon energy of approximately 890 eV (Refs. 40, 43). X-ray lasers are planned which will have a wavelength of approximately 1 Å, i.e., 12.4 keV, (Ref. 36). The interaction of X-rays with matter at these energies is controlled largely by the photoelectric effect and the Compton effect (Ref. 39). For elements with low atomic number, Z, the photoelectric effect cross sections will be dominated by the K shell transitions.

For all relevant situations at these energies, the absorption will scale directly with the atmospheric mass in the path of the X-ray beam, i.e., it is appropriate to treat the absorption by means of a scaled mass absorption coefficient. Then we have the usual differential equation for beam intensity:

$$dI/dh = \rho \mu I \qquad (1)$$

where ρ is the density of the medium in question, μ is the mass absorption coefficient, I is the beam intensity, and beam propagation is taken to be along the minus h direction, i.e., vertically downward from space to the atmosphere. The mass absorption coefficient, μ, includes both absorption by the photoelectric effect and scattering by the Compton effect. Thus, all processes removing energy from an initially collimated, monoenergetic beam are included in the definition of μ.

Cross sections for the Compton effect (scattering of X-rays off essentially free electrons) is independent of the energy of the X-ray photons. Cross sections for photoelectric absorption (neglecting variations at K shell edges which are unimportant for our application of 1 to 14 Å wavelength) scale approximately like E^{-3}, where E is the energy of the X-ray photon (Ref. 37). Therefore, photoelectric absorption will necessarily dominate at low energies.

In line with U. S. Standard Atmosphere Tables, we shall assume an effective atmospheric composition at 100 km altitude, by volume, of 78% N_2, 21% O_2, and 1% Ar, with negligible water vapor. We shall adopt a value for the scale height, H, of 6.9 km. It should be emphasized that variability by a factor of two about these values, e.g., due to solar activity, is possible (Ref. 38).

From the published literature, we can evaluate the mass absorption coefficient of air at 14 Å and at 1 Å (see Appendix).

$$\mu(14\ \text{Å}) = 1.0 \times 10^5\ \text{cm}^2/\text{g}$$

and

$$\mu(1\ \text{Å}) = 8.1\ \text{cm}^2/\text{g}$$

Both of these numbers should be regarded as having an uncertainty of $\pm$ 15%. Clearly, the absorption coefficient is several orders of magnitude greater for the lower energy 14 Å X-rays, consistent with the E^{-3} scaling above.

We take the atmospheric density as

$$\rho(h) = \rho_o \exp(-h/H) \qquad (2)$$

where ρ_o is the density at some reference altitude (100 km for present purposes), h is the height above (or below) that altitude.

If we define θ to be the angle between the incident X-ray from space and the local vertical, then we can derive from Eq. (1) the differential equation for the intensity as a function of altitude propagating from space into a plane-parallel exponential atmosphere at an angle θ,

$$(dI/dh)\cos\theta = \rho\mu I = \rho_o\mu I \exp(-h/H) \qquad (3)$$

This is a separable differential equation and easy to solve.

$$dI/I = (\rho_o\mu/\cos\theta) \exp(-h/H)dh$$

$$\ln I = \int_{\infty}^{h} (\rho_o\mu/\cos\theta) \exp(-h/H)$$

$$= (\rho_o\mu/\cos\theta)\left[-H \exp(-h/H)\right]_{\infty}^{h}$$

The resulting intensity is

$$I = I_o\exp[-(\rho_o\mu H/\cos\theta) \exp(-h/H)] \qquad (4)$$

where I_o is the incident X-ray intensity far above the atmosphere.

If we adopt the standard value of $\rho_o = 8 \times 10^{-10}$ g/cm^3 appropriate to an altitude of 100 km, we can completely determine the intensity at a given altitude in the atmosphere of an X-ray beam entering the atmosphere with a slant angle . Figures 7-1 and 7-2 are graphs of the propagation of X-rays into the atmosphere for different incident angles for X-ray wavelenghs of 14 Å and 1 Å. It is apparent that for wavelengths of 14 Å, absorption is essentially complete at an altitude between 120 and 125 kilometers, while the 1 Å X-ray beam can penetrate to altitudes of the order of 50 to 60 km X-ray beams generated at lower altitudes would be absorbed at considerably shorter distances than for sources in space.

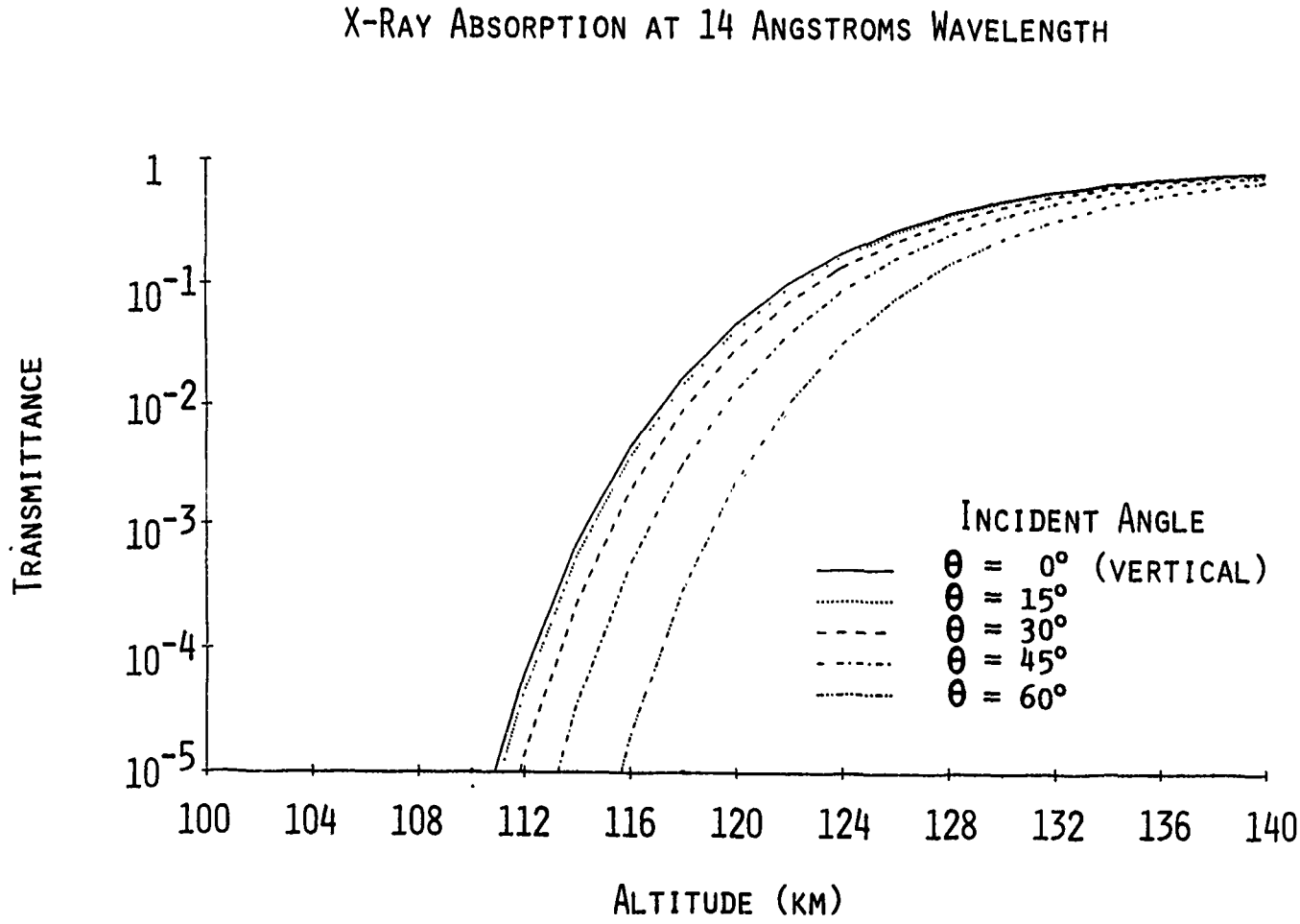

Figure 7-1. Transmission from space into the atmosphere at different incident angles for 14 Å wavelength X-rays. (Zero degrees is vertical propagation into the atmosphere.) Transmission is reduced to 10% when the beam has propagated from space to about 120 km altitude.

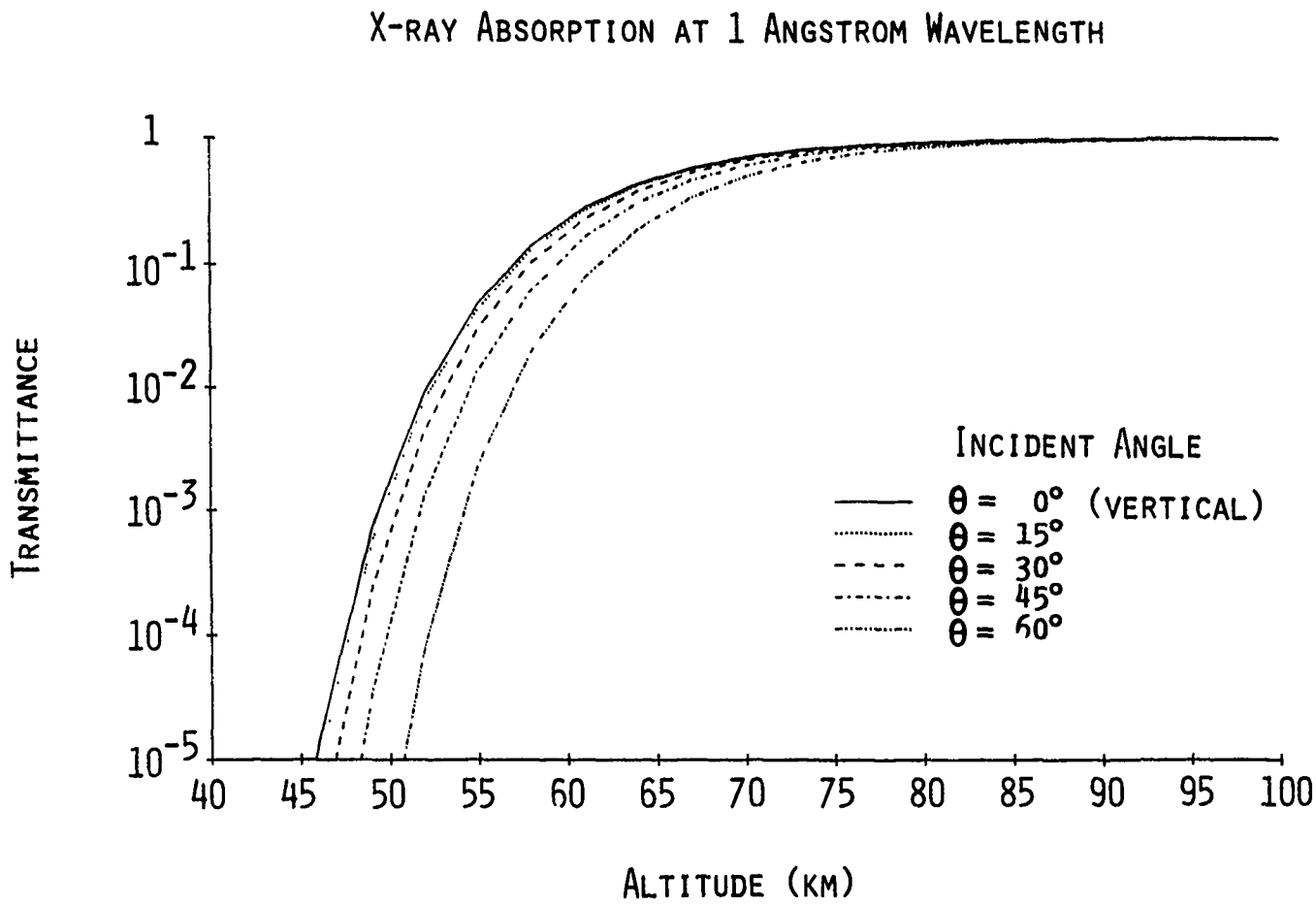

Figure 7-2. Same as Figure 7-1 except for an X-ray wavelength of 1 Å. Transmission is reduced to 10% when the beam has propagated from space to about 55 km altitude.

8. RECOMMENDATIONS

8.1 Background

The use of EM waves for communication, guidance and target recognition has long been effectively implemented in military systems. The system designs and spectral ranges used have been dictated by the atmospheric transmission windows, and governed by the availability of technology with reasonable cost and high reliability. There is, however, a need for constant improvement of these systems. In the communication area, for example, the reliable but overcrowded microwave bands no longer have sufficient channel capacity to accommodate the projected explosive increase of information transfer in digital communications. Thus the technology is being pushed towards the MMW (EHF) arena. The communications must be robust, i.e., all-weather and low-error-rate. There is also the potential development of using EM waves as directed energy weapons. Therefore, it is necessary to review from time to time the atmospheric effects on EM wave propagation in view of the changing requirements, as well as technology, and to determine if there are new opportunities in spectral ranges not currently in use.

8.2 Path Length Absorption Measurements

We recommend using horizontal path absorption studies to estimate path length absorption and degradation of satellite microwave and MMW signals.

Reception of satellite MW/MMW signals by a ground station or an aircraft (e.g., Figure 8-1) involves absorption and scattering along a slant path which traverses the whole depth of the troposphere. This implies the existence of a wide range of scattering obstacles, from oblate raindrops at positive (and sometimes negative) temperatures to ice particles of differing shapes and orientations with respect to the horizontal at lower temperatures. In order to investigate the detailed absorption and scattering of such particles, different approaches are possible. While a theoretical investigation is possible for particles of well defined geometry, and whose microwave refractive indices are known, in general the complex shapes and orientations defy a rigorous analysis. This is particularly true for the complex shapes of snowflakes and hail particles; the problem is made worse by a largely unknown size distribution, and is further compounded when regions of cloud and precipitation exist as mixed phase (liquid, gas, solid) composition. One approach to these problems has been to measure absorption along a horizontal path under conditions of somewhat uniform spatial distribution of such particles. This was the case for the SNOW field tests. Under such conditions, the precipitation can be characterized by ground surface measurement using optical or other techniques. This can, in principle, enable an empirical library to be computed

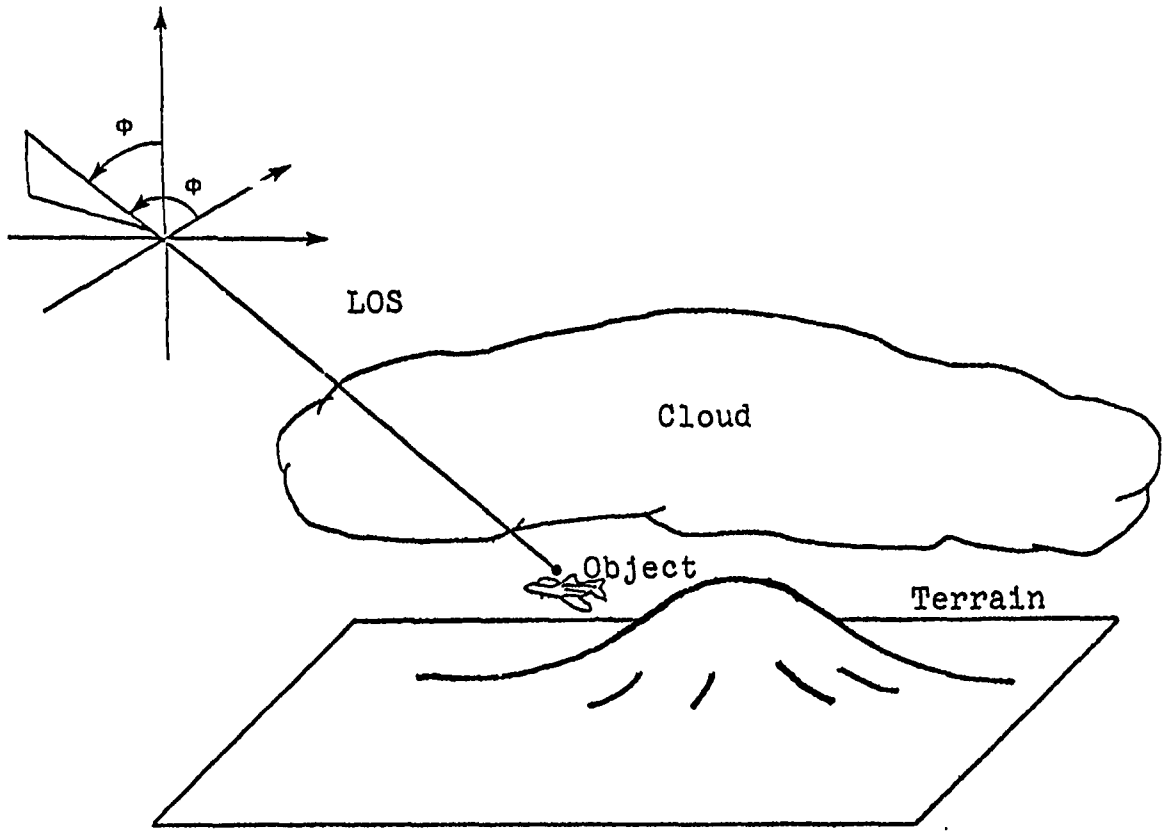

Figure 8-1. Satellite-to-Aircraft Communication Scenario.

in order to determine absorption related to a suitably cataloged, particle type, particle size, dispersion and concentration. This could then lead to the reconstruction of absorption along a slant path, bearing in mind that a considerable prediction capability might be needed for this characterization at different levels in the atmosphere.

In practice things are even more complex than outlined above--measurements at the ground characterize only limited aspects of the particles which actually occur in nature. For example, vertical velocity is necessarily very small, and it is not possible to reproduce conditions in a deep growing convective cloud. Even stratiform surface clouds (fog) will poorly reproduce the growth processes which take place in convective clouds well above the ground. The particle mix will be quite different; most important it appears that the high liquid water content found in clouds cannot be obtained near ground level even in dense fogs. This is important since the growth of the ice particles in clouds may also include a liquid coat. This means that several important situations cannot be investigated near the ground.

A possible way out of this dilemma is to carry out horizontal path measurements from two mountain top sites through precipitation falling between source and receiver. This could give useful data for stratiform/small convective clouds for mountains of a few 1000 feet high, as might occur in

the New England area. It might be of greater utility to establish a site in a deeper mountain range (e.g., the Sierra Nevada) where convection in deep valleys could be monitored as storm systems swept in from the Pacific (winter time) and during deep summer time thunderstorms convection (e.g., Puerto Rico).

8.3. Computations

We also recommend performing computations with the attenuation subroutine in conjunction with the AFGL/CSU cloud model. An important part of this computational work would be the testing of algorithms to determine attenuation versus wavelength for different weather conditions as simulated by the AFGL/CSU cloud model. These algorithms would be useful to station weather officers and other field personnel to aid in relating their field observations to expected systems performance.

There are two modes of possible operation for the attenuation subroutine: (1) it is anticipated that the subroutine would ask the AFGL/CSU model for those parameters (e.g., liquid/frozen water content) which would be needed to calculate attenuation, based on the prevailing weather conditions; or (2) the AFGL/CSU model would use the subroutine either off-line or on-line. For instance, in the off-line mode, the subroutine could be used to generate a "look-up

table" of attenuatlon values for subsequent use by the main AFGL/CSU model.

An important part of this computational work is model verification (using available data) as well as the design of the recommended field tests to fill data gaps and to extend the range of validity of the model. That is, use of the attenuation subroutine should enable the AFGL/CSU model to be applied to a variety of field sites where data are extensive on terrain factors and meteorological conditions. In this way, it should be possible to use the AFGL/CSU model to describe and/or predict mesoscale weather conditions anywhere in the world and to apply the results to the attenuation of multispectral systems.

Finally, sensitivity studies using the AFGL/CSU model with the attenuation subroutine should be run. This would allow examination of the important variables affecting cloud transmission. Ultimately, simple scaling laws may be derived from such sensitivity calculations. At that point, the scaling laws could be readily used to design and evaluate the recommended field experiments and to assist the Air Force in real-time prediction of weather effects on optical, infrared, millimeter wave, and microwave systems. A prime example is an ability to calculate and predict MMW (EHF) downtime for potential ground communication sites based on short-term variations, versus the traditional long-term variation climatological means of determining such sites.

9. REFERENCES

1. G. J. Tripoli, W. R. Cotton, "The Colorado State University Three Dimensional Cloud/Mesoscale Model, Part I, General Theoretical Framework and Sensitivity Experiments", J. Rech. Atm. 16, no. 4 (1982); and W. R. Cotton, M. A. Stephens, T. Nekrhorn, and G. J. Tripoli, "Part II: An Ice Phase Parameterization", J. Rech. Atmos. 16, no. 4 (1982).
2. L. D. Duncan and R. C. Shirkey, "EO-SAEL-82, Vol. I and II", Tech. Rpt. ASL-TR-0122 (Nov. 1982).
3. V. Falcone, private communication (1984).
4. L. J. Ippolito, "Radio Propagation for Space Communications Systems", Proc. IEEE, Vol. 69, No. 6 (June 1981).
5. R. A. McClatchey, R. W. Fenn, J. E. Selby, F. E. Volz, J. S. Garing, "Optical Properties of the Atmosphere (Revised)", Environmental Research Paper No. 354, Air Force Cambridge Research Laboratory, Bedford, MA, AFCRL-71-0279, AD726116 (May 1971).
6. S. S. Penner, Quantitative Molecular Spectroscopy and Gas Emissivities (Addison Wesley, Reading, Mass., 1959.)
7. Van de Hulst, Light Scattering by Particles (Academic, New York, 1967).
8. E. S. Rosenblum, "Atmospheric Absorption of 10 - 400 GHz Radiation", Microwave J. 1, 91 (1961).

9. V. J. Falcone, L. W. Abreu, and E. P. Shettle, "Atmospheric Attenuation of Millimeter and Submillimeter Waves: Models and Computer Code", Environmental Research Paper No. 679, Air Force Geophysics Laboratory, Bedford, MA, AFGL-TR-79-0253, ADA084485 (15 Oct. 1979).

10. P. S. Ray, "Broadband Complex Refractive Indices of Ice and Water", Appl. Opt. 11, 1836-1844 (1972).

11. W. M. Irvine and J. B. Pollack, "Infrared Optical Properties of Water and Ice Spheres", Icarus 8, 324-360 (1968). See also: J. W. Schaaf and D. Williams, "Optical Constants of Ice in the Infrared", J. Opt. Soc. Am. 63, 726-732 (1973).

12. G. M. Hale and M. R. Querry, "Optical Constants of Water in the 200-nm to 200- m Wavelength Region", Appl. Opt. 12, 555-563 (1973).

13. S. G. Warren, "Optical Constants of Ice from the Ultraviolet to the Microwave", Appl. Opt. 23, 1206-1225 (1984).

14. D. Lukes, "Penetrability of Haze, Fog, Clouds, and Precipitation by Radiant Energy over the Spectral Range 0.1 Micron to 10 Centimeters", Cent. for Naval Analyses, University of Rochester, p. 45 (May 1968).

15. J. S. Marshall and W. M. Palmer, "The Distribution of Raindrops with Size", J. Meteorology 5, 165 (1948).

16. J. O. Laws and D. A. Parsons, "The Relationship of Raindrop Size to Intensity", Trans. Am. Geophys. Union 24, 452 (1943).

17. J. Joss, J. C. Thams, and A. Waldvogel, "The Variation of Raindrop Size Distributions at Locarno", Proc. Int. Conf. Cloud Physics, Toronto, Canada, pp. 369-373 (1968).

18. H. R. Prupacher, "The Microstructure of Atmospheric Clouds and Precipitation", Clouds: Their Formation, Optical Properties, and Effects (Academic, New York, 1981), P.B. Hobbs and A. Deepak, eds.

19. S. K. Cox, "Radiation Characteristics of Clouds", Clouds, Their Formation, Optical Properties, and Effects (Academic, New York, 1981), P. B. Hobbs and A. Deepak, eds.

20. J. Hallett, "On the Characterization of Ice Particles in the Atmosphere", Proc. SPIE Tech. Symp. East '83 (April 1983).

21. J. B. Mason, "Light Attenuation in Falling Snow", Tech. Rpt. ASL-TR-0013, U.S. Army Atmospheric Sciences Laboratory, NM (1978).

22. W. Nakaya, Snow Crystals: Natural and Artificial (Harvard Univ. Press, Cambridge, 1954).

23. V. W. Richard (1976), as reported by G. B. Tiffany, "Most Reliable Messenger: MM-Waves Get Through", Microwaves & RF, p. 64 (Sept. 1983).

24. R. W. McMillan, J. J. Gallagher, and A. M. Cook, "Calculations of Antenna Temperature, Horizontal Path Attenuation, and Zenith Attenuation due to Water Vapor in the Frequency Band 150-700 GHz", IEEE Trans. in Microwave Theory and Techniques, Vol. MTT-25, No. 6, pp. 484-488, Id. No. 132131 (June 1977).

25. D. Deirmendjian, "Far Infrared and Submillimeter Wave Attenuation by Clouds and Rain", J. Appl. Meteorol. 14, 1584-1593 (1975).

26. S. H. Lin, H. J. Bergman, and M. V. Pursley, "Rain Attenuation on Earth Satellite Paths--Summary of 10 Years Experiments and Studies", Bell Syst. Tech. J., 59, no. 2, 183-228 (Feb. 1980).

27. W. L. Mowland, R. L. Olson, and I. P. Shkarofsky, "Theoretical Relationship Between Rain Depolarization and Attenuation", Electronic Lett. 13, No. 22, 676-678 (1977).

28. T. S. Chu, "Rain-Induced Cross-Polarization at CM and MM Wavelengths", Bell Syst. Tech. J. 53, no. 8, 1557-1559 (1974).

29. C. W. Bostian and J. E. Allnutt, "Ice Crystal Depolarization on Satellite-Earth Microwave Radio Paths", Proc. IEEE 126, no. 10, 951-960 (Oct. 1979).

30. W. J. Vogel, "CTS Attenuation and Cross-Polarization Measurements at 11.7 GHz", U. of Texas at Austin, Austin, TX, Report no. 22576-1 (June 1980).

31. D. M. J. Devasirvathm and D. B. Hodge, "Amplitude Scintillations of Earth-Space Propagation Paths at 2 and 30 GHz", Ohio State Univ. Tech. Report 4299-4, Contract NASA-22575 (March 1977).

32. L. J. Ippolito, "ATS-6 Millimeter Wave Propagation and Communications Experiments at 20 and 30 GHz", IEEE Trans. Aerospace Electronics Syst. Vol. AES-11 (Nov. 1975).

33. D. D. Cox, H. W. Arnold and R. P. Peck, "Phase and Amplitude Dispersion for Earth-Satellite Propagation in the 20 to 30 GHz Frequency Range", IEEE Trans. Antenna Propagation, Vol. AP-28 (May 1980).

34. L. J. Ippolito, "11.7 GHz Attenuation and Rain Rate Measurements with the Communications Technology Satellite (CTS)", NASA Tech. Mem. 80283, Goddard Flight Space Center (1979).

35. H. L. Anderson, ed., 1981, Physics Vade Mecum (American Institute of Physics, New York).

36. C. G. Baldwin, J. C. Solem, and V. I. Gol'danskii, 1981, "Approaches to the Development of Gamma Ray Lasers", Rev. Mod. Phys. 53, 687-744 (1981).

37. R. L. Brown, and R. J. Gould, 1970, "Interstellar Absorption of Cosmic X-Rays", Phys. Rev. D,1, 2252-2256 (1970).

38. A. D. Danilov, Chemistry of the Ionosphere, (Plenum Press, New York and London, 1970.

39. R. Giaconni, and H. Gursky, eds., X-Ray Astronomy (D. Reidel Publishing Co., Dordrecht-Holland, 1974).

40. J. Hecht, Beam Weapons: The Next Arms Race (Plenum Press, New York and London, 1984).

41. B. L. Henke and R. L. Elgin, Adv. X-Ray Analysis, 13, 639 (1970).

42. S. Jornu, "X-Ray Laser Applications Study", (Physical Dynamics, Inc., La Jolla, CA, report PD-LJ-77-159, 1977).

43. C. A. Robinson, "Advances Made on High-Energy Lasers", Aviation Week & Space Technology (Feb. 23, 1981).

44. R. D. Hill, "Lightning-Induced by Nuclear Bursts", J. Geophys. Res. 78, 6355-6358 (1973).

APPENDIX. X-RAY ABSORPTION COEFFICIENT OF AIR

For the purposes of this discussion, we adopt the fractional compositions of our three atmospheric components, nitrogen, oxygen, and argon (water vapor is negligible at altitudes greater than 50 km):

$f_N = 0.78 \quad f_O = 0.21 \quad f_{Ar} = 0.01$

each with a molecular weight

$M_N = 28.01 \quad M_O = 32.00 \quad M_{Ar} = 39.95$

Here, we assume that the X-ray absorption coefficient per molecule is simply the sum of the absorption coefficients per atom. We define μ_i as the mass absorption cross section, in cm^2/g of species i. Then, the mass absorption coefficient for air is

$$\mu_{air} = (f_N M_N \mu_N + f_O M_O \mu_O + f_{Ar} M_{Ar} \mu_{Ar})/(f_N M_N + f_O M_O + f_{Ar} M_{Ar})$$

For 14 Å X-rays, we adopt the measured absorption coefficients from Ref. 41:

$\mu_O = 6.5 \times 10^4 \ cm^2/g$

$\mu_N = 4.9 \times 10^4 \ cm^2/g$

$\mu_{Ar} = 4.1 \times 10^3 \ cm^2/g$

For 1 Å X-Rays, we take values from (Ref. 37) (with slight extrapolation required):

$\mu_O = 4.68 \ cm^2/g$

$\mu_N = 2.20 \ cm^2/g$

$\mu_{Ar} = 2.75 \ cm^2/g$

and so for 14 Å X-rays

$$\mu_{air} = 1.04 \times 10^5 \text{ cm}^2/\text{g}$$

and for 1 Å X-rays

$$\mu_{air} = 8.12 \text{ cm}^2/\text{g}$$

Printed by
United States Air Force
Hanscom AFB, Mass. 01731